NATIONAL ADVISORY COMMITTEE FOR AERONAUTICS

TECHNICAL NOTE 3786

HANDBOOK OF STRUCTURAL STABILITY

PART VI - STRENGTH OF STIFFENED CURVED PLATES AND SHELLS

By Herbert Becker

New York University

Washington
July 1958

TABLE OF CONTENTS

NATIONAL ADVISORY COMMITTEE FOR AERONAUTICS

TECHNICAL NOTE 3786

HANDBOOK OF STRUCTURAL STABILITY

PART VI - STRENGTH OF STIFFENED CURVED PLATES AND SHELLS

By Herbert Becker

SUMMARY

A comprehensive review of failure of stiffened curved plates and shells is presented.

Panel instability in stiffened curved plates and general instability of stiffened cylinders are discussed. The loadings considered for the plates are axial, shear, and the combination of the two. For the cylinders, bending, external pressure, torsion, transverse shear, and combinations of these loads are considered.

General instability in stiffened cylinders was investigated. For bending and torsion loads, test data and theory were correlated. For external pressure several existing theories were compared. As a result of this investigation a unified theoretical approach to analysis of general instability in stiffened cylinders was developed.

INTRODUCTION

The objective of this part of the "Handbook of Structural Stability" is to continue the comprehensive survey of the field of instability by a review of theory and data pertaining to failure by buckling of stiffened curved plates and shells.

The literature on general instability of stiffened cylinders consists of experimental data obtained by some investigators and theory devised by others particularly under bending loads. However, in no case was correlation of the two obtained. Consequently, at present, only empirical data are available to engineers. A sound mathematical foundation, correlated with theory, does not exist. However, effecting this correlation appears to be possible by use of the published literature, and therefore a major portion of this report is devoted to an attempt to effect such correlation.

In order to obtain a proper perspective on instability of shells it appears pertinent to review briefly the field of structural stability as contained in the preceding parts of this Handbook (refs. 1 to 5). Comparison of the buckling stress with experimentally determined values has yielded good correlation for flat and curved plates, separately or in combination, in a variety of loading conditions in both the elastic and inelastic stress ranges (Parts I, II, and III, refs. 1, 2, and 3, respectively). However, attempts to apply extensions of this approach to calculation of failure in unstable elements have been relatively unsuccessful. An effective semiempirical approach to this problem is described in Parts IV and V (refs. 4 and 5, respectively).

For some types of structures, such as flat plates, the failing load may exceed the buckling load by a large percentage. In Part III (ref. 3) this was ascribed to the induction of tensile membrane stresses in the plate, at large deflections, which presumably act to restrain postbuckling deflections. For axially compressed isotropic cylinders, however, the induced membrane forces would be compressive and consequently would tend to generate an unstable postbuckling condition. This would cause buckling and failure to be coincident. When the membrane forces are neutral, as in isotropic cylinders in torsion or under inward pressure, buckling and failure would tend to be coincident.

When these considerations are extended to stiffened cylinders, it appears reasonable to anticipate equality of buckling and failure stresses for those designs in which panel instability is avoided. However, if panel instability should occur first, the cylinder may continue to carry load until the frames fail, in which case the failure stress could exceed the buckling stress.

At present, the experimental data on failure of stiffened curved plates and shells are correlated with empirical methods of analysis. In this report, the correlation of general instability data with theory is presented. The analytic procedure involves the use of differential equations employing solutions based on observations of structural behavior during tests. A discussion of the modes of failure encountered in stiffened curved plates and shells is presented in the section entitled "Review of Existing Data."

The strength of stiffened curved plates, which relates principally to panel instability, is discussed in the section entitled "Strength of Stiffened Curved Plates." The remainder of the report deals with general instability of stiffened shells.

The last comprehensive survey of the background of the field of general instability was presented by the Guggenheim Aeronautical Laboratory, California Institute of Technology, (GALCIT) under the sponsorship of the National Advisory Committee for Aeronautics (refs. 6 to

14). Since then a large mass of theoretical and experimental data has been published, such as the work done by the Polytechnic Institute of Brooklyn, Aeronautical Laboratory (PIBAL) (refs. 15 to 25). The history of the field is brought up to date in the section entitled "Review of Existing Data," which includes an evaluation of the state of the art up to the present time.

In the past the major investigative effort in the field of general instability was focussed on the problem of bending of stiffened circular cylinders. This topic is discussed in the section entitled "Bending General Instability," which contains data for designing to avoid bending general instability. In aircraft construction this type of general instability is the one most likely to occur out of the various types possible, and consequently it is feasible to consider the possibility of optimum design for bending. This is discussed in the section entitled "Optimum Design for Bending."

The effect of cutouts upon the general instability stress of a stiffened circular cylinder is examined in the section entitled "Cutout Cylinders in Bending General Instability," in which a simplified approach to the analysis of symmetric cutouts is described. The theories relating to general instability under external pressure are reviewed in the section entitled "Pressure General Instability."

The general instability under shear loadings is described in the section entitled "Torsion General Instability," which relates to torsion loads, and in the section entitled "Transverse-Shear General Instability," which applies to transverse shear. Test data are compared with theory for torsion loads to find the relative strengths under torsion and shear loadings. Interaction under combined torsion and bending is discussed in the section entitled "Combined Bending and Torsion Instability."

The state of the art is reviewed in the last section in the light of the data contained in this report. On the basis of this evaluation it is possible to make recommendations for applications of the data to design and analysis of stiffened curved plates and shells. The procedures to be followed are described in the appendix.

This survey was conducted at New York University under the sponsorship and with the financial assistance of the NACA and under the direction of Dr. George Gerard.

SYMBOLS

A_f	area of frame, sq in.
A_s	area of stiffener, sq in.

b	stiffener spacing, in.
b'	effective span of frame for inward-bulge buckling (fig. 2 in.
C	coefficient in modified classical equation for axial compression buckling of isotropic cylinder
C_1, C_2	parameters in orthotropic-buckling-stress equation
c	end-fixity coefficient for axially compressed stiffeners $(d/L')^2$
c_δ	coefficient in frame-spring-constant expression
D	diameter, in.
d	frame spacing, in.
E	modulus of elasticity, psi
e	eccentricity of frame centroid from center of sheet, in.
F	parameter of stiffened cylinders for external-pressure general instability
G	shear modulus of elasticity, $E/[2(1 + \nu)]$, psi
g	parameter in expression for bending general instability stress
I_f	distributed bending moment of inertia of frame, $\bar{I}_f/d$, cu in.
I_s	distributed bending moment of inertia of stiffener, $\bar{I}_s/b$, cu in.
$\bar{I}_f$	bending moment of inertia of frame, $in.^4$
$\bar{I}_s$	bending moment of inertia of stiffener, $in.^4$
I_{NA}	moment of inertia of cutout cylinder cross section about neutral axis, $in.^4$

I_{xx}	moment of inertia of cutout cylinder cross section about horizontal diameter, in.^{4}
J	$J_f + J_s$, cu in.
J_f	distributed torsional moment of inertia of frame, $\bar{J}_f/d$, cu in.
J_s	distributed torsional moment of inertia of stiffener, $\bar{J}_s/b$, cu in.
$\bar{J}_f$	torsional moment of inertia of frame, in.^{4}
$\bar{J}_s$	torsional moment of inertia of stiffener, in.^{4}
K_f	frame spring constant per inch of effective span, $P/b'\delta$, psi
k_p	buckling-stress coefficient for hydrostatic inward pressure
k_t	buckling-stress coefficient for torsion
k_y	buckling-stress coefficient for radial inward pressure
L	length of cylinder, in.
L'	effective length of axially compressed stiffener (fig. 2), in.
M	bending moment, in-lb
M_o	bending moment in uncut cylinder at general instability, in-lb
m	axial waveform parameter
N_x	axial applied loading, lb/in.
N_{xy}	shear applied loading, lb/in.
N_y	applied circumferential loading, lb/in.

n	circumferential waveform parameter
P	concentrated radial load applied to frame to determine effective spring constant, lb
P_{cr}	critical axial load for stiffener, lb
p	pressure loading, psi
Q_b	parameter for bending general instability
$Q_t, Q_t', \bar{Q}_t$	parameters for torsional general instability
R	cylinder radius, in.
R_p, R_q	shear- and compression-stress ratios
T	torque, in-lb
T_o	torque at general instability, in-lb
t	thickness of sheet, in.
t_e	equivalent sheet thickness, in.
t_f	distributed frame area, A_f/d, in.
t_s	distributed stiffener area, A_s/b, in.
$\bar{t}$	effective thickness of sheet for shearing rigidity, in.
V	shear load, lb
v	tangential displacement, in.
$W, \bar{W}$	frame stiffness parameters (eqs. (22) and (23))
w	radial displacement, in.
w_e	effective width of sheet per side of stiffener, in.
w_o	maximum radial displacement on inward-bulge buckle, in.
x, y	axial and tangential coordinates, in.
$\bar{y}$	distance from coordinate fiber to centroidal axis, in.

Z, Z_o	section modulus for cut and uncut cylinders, cu in.
Z_L	cylinder curvature parameter, $(L^2/Rt)(1 - \nu^2)^{1/2}$
Z_b	plate curvature parameter, $(b^2/Rt)(1 - \nu^2)^{1/2}$
$\bar{z}$	distance to neutral axis of frame plus effective sheet measured from sheet center, in.
α	half angle of cut cylinder, radians
α_p	panel efficiency coefficient
β	parameter related to wave-length ratio, n/m
δ	radial deflection of frame under concentrated radial load, in.
Σ	solidity
η	plasticity-reduction factor
θ	angle of cutout, radians
Λ_o	parameter for evaluating bending general instability
ν	Poisson's ratio for isotropic structures
ν_{xy}, ν_{yx}	x and y Poisson's ratios for orthotropic structures
ρ_f	frame section radius of gyration, in.
ρ_s	stiffener section radius of gyration, in.
σ	stress, psi
σ_c	compressive stress at bending general instability, psi
σ_{cr}	compressive buckling stress of sheet, psi
σ_y	circumferential normal stress under external pressure at general instability, psi

τ, τ_t	shearing stress at torsional general instability
$\bar{\tau}$	generalized plasticity-reduction factor
τ_{cr}	shear buckling stress of sheet, psi
τ_v	shearing stress at shear general instability, psi
ϕ	general angle on cylinder cross section (fig. 2), radians
ϕ_o	angle to terminus of inward bulge (fig. 2), radians

Subscripts:

o	optimum design
av	average
c	compression
cy	compressive yield
f	pertaining to frame
s	pertaining to stiffener
y	y-direction

REVIEW OF EXISTING DATA

Introduction

The present knowledge concerning the failure of stiffened curved plates and shells is difficult to apply to engineering problems. Not only are there discrepancies between theory and test data, but in the case of bending of stiffened cylinders, for example, two different sets of test data are in conflict.

As a prelude to the analysis of the existing data, which is the intent of this report, a review of these data appears in this section. The modes of instability are described, and a historical review of the theoretical and experimental data relating to general instability is presented. The information in this review permits an assessment of the state of the art in applying data on general instability to the solution

of engineering problems. The deficiencies in the present state of the art are listed in summary form.

The emphasis of the present report is derived from this evaluation and is described at the end of this section.

Instability Modes

The buckling and failure of stiffened flat plates are described in Parts II and V of this Handbook (refs. 2 and 5, respectively), in which the nature of instability in the stiffeners and sheet is described. In the approach employed in the analysis the principal load-carrying structure is considered to be restrained by deflectional and rotational springs representing the supporting structure. The details of this method of analysis were presented in Part V (ref. 5). The report by Budiansky, Seide, and Weinberger may be consulted for examples of application of this approach to elastically supported columns (ref. 26). This method was also used extensively by Gerard in the analysis of optimum design in compression structures (ref. 27). For detailed treatments of this spring-support approach, references 5 and 27 should be consulted. Results of these investigations have been excerpted here to depict the different modes of failure to be anticipated in stiffened-sheet construction.

When a stiffened sheet is bent into an arc so that it conforms to the surface of a cylinder, the curvature may affect the instability behavior under different types of loading. Nevertheless the manner in which buckling can occur in the curved stiffened sheet may be classified as panel instability, general instability, or optimum instability. The details of these types of instability are described in the following sections.

Panel instability.- Panel instability is generally restricted to panels that buckle between two adjacent frames. It is depicted for axial load in figure 1(a), together with the corresponding spring behavior. For purposes of illustration, only deflectional-type springs are considered, and consequently the axial stiffeners behave as pinned columns with a length equal to the frame spacing. If the springs were to have rotational rigidity, there would be a certain amount of fixity applied to the stiffeners at the frames. This model is utilized in reference 5 for flat stiffened plates.

Under panel instability, the axial stiffeners and sheet would tend to deflect primarily in a radial direction with little tendency for tangential motion.

The influence of curvature on the panel instability of stiffened plates is discussed in the section entitled "Strength of Stiffened Curved Plates."

General instability.- For panel instability the transverse stiffeners are required to have a spring stiffness at least great enough to enforce nodes in the axial stiffeners at the frames. Any deflectional stiffness in excess of this amount does not contribute to additional buckling strength. General instability may occur when the spring constant of the frames is less than this minimum value. The behavior of such a cylinder in bending is depicted in figure 1(b). Instability is no longer confined to the region between adjacent frames but may extend over several frame spacings.

This behavior is typical of axially loaded stiffened cylinders or of stiffened cylinders in bending. It is possible to design a shell which is satisfactory for external pressure by utilizing circumferential stiffeners only. In this case buckling of the frames constitutes general instability. An approach to the analysis of general instability in stiffened cylinders through use of a Donnell type equation (ref. 28) has been employed by several investigators. The eighth-order partial-differential equation for analyzing general instability is presented in the section entitled "Bending General Instability." Instability stresses are found from solutions of this equation which satisfy the cylinder boundary conditions.

The buckle shapes for unstiffened cylinders under various loadings are described in reference 3. The waveforms for stiffened cylinders correspond, more or less, to these shapes for the corresponding loadings. The largest difference occurs for cylinders in bending, while there is close similarity for torsion and external pressure loads.

The waveform shape for bending general instability has been described as the "inward bulge." The geometry of this shape, as utilized by Hoff in the analysis of this type of general instability (refs. 29 and 30), is depicted in figure 2. It consists, primarily, of a single buckle located midspan at the extreme compression fiber. The total length involved is of the order of twice the length of the buckle shape which one of the cylinder axial stiffeners would assume under the compressive failure stress of the cylinder. The inward bulge of the frame at the extreme bending fiber of the cylinder is accompanied by a pair of outward bulges on either side together with a certain amount of circumferential displacement of the frame in the region of the node points of the circumferential waveform. This type of buckle is an approximation to the single diamond buckle observed in unstiffened cylinders in bending.

Brazier instability (ref. 31), which involves collapse of the cylinder by flattening of the cross section, is theoretically possible in

a stiffened cylinder. However, the lengths involved presumably are large compared with those encountered in a practical structure or in the test cylinders described in the literature.

The multiple-spiral wave observed in stiffened cylinders loaded to general instability in torsion is a close reproduction of the shape observed on isotropic cylinders.

Test data on stiffened cylinders loaded by external pressure have not been published. However, the wave shapes assumed for purposes of analysis resemble those employed in calculating buckling stresses in isotropic cylinders under this type of loading. These latter shapes represent observed buckle waveforms for external pressure loads.

The buckle shapes for isotropic cylinders normally would be affected by the lengths of the cylinders. For stiffened cylinders, however, the available test data pertain to cylinders which may be classified as moderate length since the slope and curvature boundary conditions do not appear to influence the buckling behavior. The two-lobed pattern to be expected in cylinders loaded in torsion was not observed, which excludes the possibility of classification as long cylinders.

Optimum mode.- One approach to the design of stiffened cylinders is based on the philosophy that general instability should be prevented and the stiffener and sheet combination should be designed on the basis of panel instability. In order to insure the stability of the frames it may be necessary to employ a factor of safety in conjunction with their design.

It is hypothetically possible to select frame proportions so that panel and general instability occur simultaneously. Since this design would lead to the lightest structural weight for the applied load, the configuration of the buckle in this condition may be said to correspond to that of the optimum mode. This requires, of course, that all the possible modes of panel instability occur simultaneously. That is, the panel is an optimum designed unit. However, since there may be varying degrees of optimum design, it may be correct to claim an optimum design for a stiffened cylinder in which panel and general instability occur together although the panel itself may not be optimum.

These considerations are applied to the case of bending of stiffened cylinders in the section entitled "Optimum Design for Bending."

Historical Review of General Instability

The fundamental theory for buckling of orthotropic cylinders was developed by Flügge as an extension of the three equilibrium equations

which he derived for isotropic cylinders (ref. 32). The orthotropic-cylinder equilibrium equations were predicated on the assumption that the wall of a practical stiffened cylinder could be assumed to act as though it had uniform section properties axially and circumferentially which were different from each other.

Solutions to Flügge's orthotropic equations were obtained by Dschou for axial loading (ref. 33). Nissen (ref. 34) and Ryder (ref. 35) modified these results for purposes of better agreement with test data and for simplicity in application.

Taylor derived an eighth-order partial-differential equation for axially loaded orthotropic cylinders (ref. 36) utilizing the simplifications employed by Donnell in the derivation of his isotropic cylinder equation. Taylor's result is the same as that of Dschou, except for the influence of Poisson's ratio which Taylor assumed to be equal to zero.

This work was all completed in the 1930's. An extensive bibliography and a detailed description of the early historical development of the field of general instability in orthotropic cylinders may be found in the first GALCIT report (ref. 6), which includes a discussion of failure by flattening (Brazier instability) together with descriptions of the general instability theories in existence at that time.

The theories of Dschou (ref. 33), Taylor (ref. 36), and Hoff (ref. 29) were compared to the few existing test data. Correlation was found to be poor, with Hoff's approach yielding stresses below the experimental values while the theories of Dschou and Taylor led to stresses several times as great as those from test. The calculations performed by GALCIT for this comparison (ref. 6) utilized the nominal section properties of the cylinder frames and stiffeners.

GALCIT followed this report with tests on more than 200 cylinders loaded in bending and in torsion. The behavior of unstiffened circular cylinders was used as a guide to derive empirical relationships with which to correlate the data. In this manner parameters were determined in terms of which the data were plotted on linear paper. The relationship between measured axial buckling strain and the derived parameter was found to be linear to a reasonably good degree of accuracy for the bending data.

During the latter part of this period PIBAL initiated a parallel program of analysis and testing (refs. 15 to 25). The theory was based upon the earlier work of Hoff (refs. 29 and 30), which was modified to yield correlation with the GALCIT bending data (refs. 7, 8, and 9). As PIBAL obtained test data (ref. 16) this approach was further modified. A later report in this series dealt with attempts to generalize the

PIBAL approach (ref. 18). The GALCIT and PIBAL test data reveal a linear relation between buckling strain and an empirical parameter derived by GALCIT, However, the PIBAL cylinders attained lower general instability stresses than did the GALCIT cylinders with the same instability parameter.

In the course of its program GALCIT again evaluated Taylor's theory by comparing its predicted general instability stress under axial compression with the general instability stress of cylinders tested in bending (ref. 10). Effective sheet was utilized by GALCIT in this comparison. Furthermore, an estimated reduction in sheet stiffness was employed in Taylor's theory for axial general instability stress. Despite these refinements Taylor's theory still predicted general-instability stress many times the test values.

The PIBAL method for analyzing bending general instability was based upon a set of curves fitted through the GALCIT test data, and consequently its validity could be tested by an independent set of data. However, when PIBAL plotted its own test data on the GALCIT chart they found an appreciable departure from the curves originally drawn through the GALCIT test points. This situation was met by altering these curves to fit the new PIBAL data. An explanation for this procedure was presented by PIBAL employing the work-energy approach originally used by Hoff together with refined estimates of the shearing rigidity of the buckled shell skin (ref. 18).

One facet of the problem of general instability of stiffened cylinders in bending which has received relatively little attention is the question of the degree of nonlinearity in the behavior of such cylinders. GALCIT stated (ref. 6) that the behavior is nonlinear. PIBAL sought to demonstrate that the cylinder behavior is essentially linear, which is the assumption implicit in the theories of Dschou and Taylor. Nobody has presented a demonstration comparable to those of Tsien (ref. 37) or Donnell and Wan (ref. 38) on the nonlinear behavior of unstiffened cylinders under axial load. As was discussed in reference 3, these approaches utilize nonlinear theory to explain the observed lowering of the axial compressive buckling stress of isotropic cylinders below that predicted by linear theory.

Both Hoff (ref. 30) and Shanley (ref. 39) determined the minimum frame rigidity necessary to prevent general bending instability in a cylinder with a particular arrangement of axial stiffeners and sheet.

Previous investigations into general instability of stiffened cylinders under external pressure have been confined to ring-stiffened shells. These consist of mathematical analyses by solution of differential equations (Flügge, ref. 32, and Bodner, ref. 40) and through the use of energy methods (Salerno and Levine, ref. 41, and Kendrick, ref. 42). Recently Becker analyzed buckling under external pressure on

cylinders with both axial and circumferential stiffening (ref. 43). No test data are available to check the predictions of these various theories.

The behavior of ring-stiffened cylinders in torsion was investigated analytically by Stein, Sanders, and Crate (ref. 44). GALCIT performed tests (reported by Dunn, ref. 13) on cylinders with axial and circumferential stiffening, for which case both Hayashi (ref. 45) and Becker (ref. 43) derived the general instability stress mathematically. A parameter was derived at GALCIT and was plotted against applied shearing stress; it was found that a linear relation existed at low elastic stress levels (ref. 13).

Current State of the Art

To summarize the state of knowledge:

(1) A large mass of test data is available on general instability of cylinders under bending and torsion loads.

(2) For bending, both GALCIT and PIBAL test data yield linear relationships between failure strain and the GALCIT empirical parameter for this case, although the two lines have different slopes.

(3) For torsion, the GALCIT test data yield a linear relationship between failure strain and the GALCIT parameter for this case at low elastic failure strains.

(4) Mathematical theories for axial buckling predict general-instability stresses several times as great as the test values for bending.

(5) Mathematical theories exist for general instability under external pressure. However, no published test data are available with which to compare them.

(6) There are differing views on the amount of nonlinearity associated with bending instability of stiffened circular cylinders.

Emphasis of Present Investigation

This report is devoted primarily to an examination of the methods for predicting bending and torsional general instability in stiffened circular cylinders. In addition, various theories on buckling under pressure loading are compared.

The principal targets are the apparent lack of agreement between mathematical theory and test data and the difference between the GALCIT and PIBAL test data, for bending loading. These discrepancies appear to be attributable to the choice of section properties to be used in Taylor's theoretical buckling stress expressions. The primary problems, in this regard, seem to be the selection of effective values for the torsional rigidities of the axial and circumferential stiffeners and the shear rigidity of the sheet. The frame stiffness criteria of Hoff and Shanley are also discussed. Lack of suitable data prevents an examination of the question of nonlinearity.

The results obtained from the various theories for general instability of ring-stiffened cylinders under external pressure are compared to determine the range of predicted stresses. The GALCIT test data for moderate-length cylinders in torsion are compared with the explicit theoretical result obtained in reference 43.

As will be seen in the section on torsion general instability, a theoretical approach leads to an expression for the instability stress that agrees with test data. There is also a theory available for general instability under external pressure for which case experimental data are not available. In the case of bending general instability, comparison of the theory of Taylor with a large amount of test data has revealed poor agreement. The principal effort in the section entitled "Bending General Instability" is devoted to a critical examination of the test data and of Taylor's theory to determine whether inconsistencies exist. If Taylor's theory can be shown to agree with test data, then a unified treatment of general instability is possible since the differential equations employed for bending, pressure, and torsional general instability are virtually the same. It would then remain to obtain test data on pressure general instability for correlation with theory.

STRENGTH OF STIFFENED CURVED PLATES

Introduction

Panel instability can occur in stiffened curved plates in any of the mode shapes pertaining to stiffened flat plates. As has been suggested previously, reference should be made to Part V (ref. 5) for a detailed discussion of this latter case for axial loading.

In this portion of the report panel instability is discussed for axial compression and shear loadings on stiffened curved plates. Each type of loading is discussed separately, after which interaction between these two loadings is described.

Axial Compression

When the strength of a flat stiffened panel is known, then it is possible to select transverse stiffening to support the panel over any specified length. One approach to this procedure is through the assumption that the transverse ribs act as deflectional and rotational springs. When the minimum required spring constant is found the ribs can be designed.

The proportions of the sheet and stiffeners are selected from data on the buckling stress and failure of curved webs and on the buckling stress and failure of stiffeners, which may be found in references 1 to 4. The frame requirements may be satisfied with the aid of the data presented in the section entitled "General Instability."

When a flat panel is bent to a circular curve the buckling stress of the sheet is increased. This leads to an increased effective width of sheet acting with each stiffener, which tends to alter its column strength. This effect is small for practical structural proportions, and the net gain in load-carrying capacity of a curved stiffened sheet is little different from that of the corresponding flat sheet. This result is demonstrated by Sechler and Dunn (ref. 46), who used the flat-sheet buckling stress to determine w_e. Their calculations of ultimate load-carrying capacity of stiffened curved sheet panels agreed fairly well with data from 32 tests covering a large range of panel curvatures.

The relative insensitivity of panel instability stress to the effect of curvature is apparent from figure 3, in which data obtained by Ramberg, Levy, and Fienup (ref. 47) are shown. The ratio of curved- to flat-panel failure stresses is plotted as a function of the curvature parameter $Z_b = b^2/Rt$. The change in failure stress is seen to be small, on the average, and appears to decrease with increasing curvature.

Additional data are provided by Sechler and Dunn (ref. 46). However, the scatter is large, and the end-fixity data are not included. Consequently, although an increasing trend of failure stress with Z_b is indicated, it cannot be evaluated accurately.

It must be noted that there is a serious need for test data on curved stiffened panels in current use.

Shear

The analysis of stiffened curved plates and shells in shear was developed by Kuhn and his collaborators at the NACA through the

modification of pure tension field theory by means of the reduction of test data. This has resulted in a semiempirical method of analysis described by Kuhn and Griffith (ref. 48).

The analysis devised by Kuhn and Griffith involves a sequence of computations which require special charts that include the effect of R/t, τ_{cr}/τ, and the stiffener and frame section properties. That report should be consulted for a description of this method and for a summary of the test data upon which it is founded.

Combined Shear and Axial Compression

The failure of curved stiffened sheet under combined axial compression and shear was investigated by Melcon and Ensrud (ref. 49). By means of an experimental program on J-stiffened panels of different sheet thicknesses, they obtained curves of shear loadings as a function of axial loading at failure.

When these results are nondimensionalized for use in stress-ratio form, it is found that an interaction equation

$$R_p + R_q^2 = 1 \tag{1}$$

is a good approximation to the data, as shown in figure 4 which includes Peterson's test data (ref. 50). It should be noted, however, that this result pertains to stiffener failure. A few panels tested by Melcon and Ensrud failed by web fracture and consequently did not attain the loading required to permit use of equation (1). For these cases it was necessary to extrapolate the curves of Melcon and Ensrud to determine the shear flow at failure when no axial loading was present.

BENDING GENERAL INSTABILITY

Introduction

In the region of the buckle that is generated when bending general instability occurs in a stiffened circular cylinder, the predominant stress is axial compression. For this reason the Taylor theory for axial-compression general instability (ref. 36) has been utilized by GALCIT and PIBAL in attempts at correlation with test data on bending general instability. Except for a few isolated cases no axial data exist with which to compare this theory. However, the close relationship between axial compression and bending behavior of isotropic cylinders

suggests the comparison of the axial-compression theory with the extensive data obtained from bending tests of stiffened cylinders. The data recorded by GALCIT and PIBAL are presented in references 7 to 18 and are not reproduced here.

As was stated in the section entitled "Review of Existing Data," the discrepancy between axial theory and bending test data was found to be large. An investigation into the possible reasons for this discrepancy indicated that the choice of stiffener and frame torsional rigidities and the shear rigidity of the sheet covering of the cylinders may have been inaccurate. An evaluation of the pertinent section properties for this type of loading is presented herein.

This revised view of the significant section properties is employed in evaluating the applicability of Taylor's theory to prediction of bending general instability in stiffened cylinders. The utility of the approach devised by Hoff (ref. 30) is also described. These two approaches represent the two theories available at present. A brief discussion is included on Brazier type instability in stiffened cylinders, which was investigated by Heck (ref. 51).

The empirical approaches of GALCIT and PIBAL are described. In addition, a new method of analysis based upon the observed physical behavior of a stiffened cylinder in bending general instability is presented utilizing the elastic-spring-support model as a basis from which to derive an expression for the bending general instability stress.

These three approaches (theoretical, empirical, and physical) comprise a comprehensive review of the field of bending general instability in stiffened circular cylinders. However, on the basis of this review conclusions cannot be drawn about the reliability of any of these methods for analyzing or designing. This is the result of the inconsistency in the test data. Consequently, the work described in this section represents an exploration of the possibilities for obtaining agreement of theory with test data with the hope that the results will have heuristic value for future investigations, which are sorely needed.

Theoretical Approach

Basic differential equation.- Taylor combined the compatibility equation for forces in the plane of a flat plate with the equilibrium equation for forces normal to the surface of a small cylinder element and obtained an eighth-order partial differential equation (ref. 36) similar to that derived by Donnell for isotropic shells. The details

of this derivation are presented in reference 43, in which this approach is extended to include the effects of shear and circumferential normal forces. The resultant equation, which is based upon an assumed zero value of Poisson's ratio, is

$$\left(\frac{1}{t_f}\frac{\partial^4}{\partial x^4} + \frac{E}{G\bar{t}}\frac{\partial^4}{\partial x^2\partial y^2} + \frac{1}{t_s}\frac{\partial^4}{\partial y^4}\right)\left[I_s\frac{\partial^4}{\partial x^4} + \frac{GJ}{E}\frac{\partial^4}{\partial x^2\partial y^2} + I_f\frac{\partial^4}{\partial y^4} + \frac{1}{E}\left(N_x\frac{\partial^2}{\partial x^2} + 2N_{xy}\frac{\partial^2}{\partial x\,\partial y} + N_y\frac{\partial^2}{\partial y^2}\right)\right](w) + \frac{1}{R^2}\frac{\partial^4 w}{\partial x^4} = 0 \tag{2}$$

The geometry of a stiffened cylinder is depicted schematically in figure 5.

Taylor solved equation (2) for axial load and found the critical axial stress in the form described below. Hayashi used a variation of equation (2) to analyze orthotropic cylinders in torsion (ref. 45), Bodner used another form to investigate external pressure on frame-stiffened cylinders (ref. 40), and Becker (ref. 43) utilized equation (2) to find explicit expressions for the general instability stress for stiffened cylinders under each of these loadings. The results of these investigations are described in this and subsequent sections.

Taylor's theory.- The expression for σ_c obtained by Taylor is

$$\sigma_c = \frac{2E}{Rt_s}\left(\frac{\beta^2 I_f + \frac{GJ}{2E}}{\frac{\beta^2}{t_s} + \frac{E}{2G\bar{t}}}\right)^{1/2} \tag{3}$$

where

$$\beta^2 = \frac{n^2}{m^2} = C_1 + \left(C_1^2 + C_2\right)^{1/2} \tag{4}$$

and

$$C_1 = \frac{\bar{t}}{2t_f}\left(\frac{t_f I_s - t_s I_f}{t_s I_f - \frac{2G^2\bar{t}J}{E^2}}\right) \tag{5}$$

$$C_2 = \frac{t_s}{t_f}\left(\frac{t_f I_s - \frac{G^2\bar{t}J}{E^2}}{t_s I_f - \frac{G^2\bar{t}J}{E^2}}\right) \tag{6}$$

This result is discussed later in this section after the test data and other theories have been described.

The half wave lengths are π/m and π/n in the longitudinal and circumferential directions, respectively. They involve the cylinder structural parameters as well as the geometric parameters and are given as follows:

$$\left.\begin{aligned} \frac{\pi}{m} &= \pi R^{1/2}\left[\left(I_s + \frac{\beta^2 GJ}{E} + \beta^4 I_f\right)\left(\frac{1}{t_f} + \frac{\beta^2 E}{G\bar{t}} + \frac{\beta^4}{t_s}\right)\right]^{1/4} \\ \frac{\pi}{n} &= \pi R^{1/2}\beta^{-1}\left[\left(I_s + \frac{\beta^2 GJ}{E} + \beta^4 I_f\right)\left(\frac{1}{t_f} + \frac{\beta^2 E}{G\bar{t}} + \frac{\beta^4}{t_s}\right)\right]^{1/4} \end{aligned}\right\} \tag{7}$$

These are continuous sinusoidal waves, the proportions of which presumably may be determined theoretically.

Hoff's theory.- Hoff investigated the general instability of stiffened circular cylinders in bending utilizing the energy method (refs. 29 and 30). The wave pattern was assumed to be an inward bulge with the proportions shown in figure 2. The theoretical expressions for the tangential and radial displacements are

$$v = \frac{w_o}{8n}\left(1 - \cos\frac{\pi x}{L'}\right)(2 \sin n\phi + \sin 2n\phi) \tag{8}$$

$$w = \frac{-w_o}{4}\left(1 - \cos\frac{\pi x}{L'}\right)(\cos n\phi + \cos 2n\phi) \tag{9}$$

with the limitation

$$\phi = \phi_o = \frac{\pi}{n} \tag{10}$$

The value of n is obtainable from test data.

The buckling stress was found by minimization of the energy increment in the usual manner. By means of a few simplifications, the length of the bulge can be eliminated from the buckling stress expression leaving only n as the parameter of interest. The buckling stress then becomes

$$\sigma_c = n^2\pi^2 E \frac{\rho_s \rho_f}{R^2}\left(\frac{t_f}{t_s}\right)^{1/2} \tag{11}$$

in which ρ_s, ρ_f, t_s, and t_f include effective sheet.

In reviewing Hoff's development, it may be seen that he first selected a value of n equal to 3 and attempted to obtain correlation with the GALCIT data. In general, the agreement was unsatisfactory. This lack of agreement was charged to uncertainties in the determinations of both internal energy in the sheet and the values of n. Subsequent reports by PIBAL discussed this problem. However, these solutions are difficult to apply to specific designs because of the implicit form of the mathematical result. Furthermore, these more detailed theories were compared with only a few test specimens, and consequently the general applicability of the method is not known.

The extension of this method of analysis by a semiempirical approach is described subsequently.

Brazier instability.- The type of general instability due to cross-section flattening of long cylinders in bending was analyzed by Brazier for isotropic circular shells (ref. 31) and by Heck for isotropic elliptic shells (ref. 51). However, no substantiating test data have been found. The results of these investigations are described in Part III (ref. 3). The failing stress of a stiffened ellipse based on small-deflection theory is

$$\sigma_c = 0.314(1 - \nu^2)^{-1/2} E \frac{t}{r}\left(\frac{t}{t_s}\right)^{1/2} \tag{12}$$

in which r is the radius of curvature of the ellipse at the extreme compression fiber.

Heck also evaluated the effect of large deflections and found that the coefficient in equation (12) increased from 0.314 to 0.39. No data are available to check these results.

Empirical Approach

GALCIT.- When GALCIT began its experimental program on general instability in stiffened circular cylinders there was little in the way of theory to serve as a guide. Consequently, tests were conducted to determine the behavior of the frame and stiffener systems with no bracing in the panels, with diagonal wire bracing in the panels, and with continuous sheet covering over the entire cylinder.

Large differences were observed in the buckling stresses for these three types of cylinders, and only the last type was analyzed by means of an empirical approach since buckling stresses for the wire-braced specimens averaged low by a factor of 2 compared with those observed for the sheet-covered cylinders, while the two unbraced specimens buckled at still lower stresses. The comparative results may be seen in figure 6.

By means of dimensional analysis in conjunction with the behavior of unstiffened circular cylinders as a guide, GALCIT derived a nondimensional parameter Q_b with which to correlate their test data. This parameter is discussed in the section on test data.

PIBAL.- The emphasis in the semiempirical PIBAL approach was concentrated upon determining the buckle waveform. As mentioned previously, Hoff proposed the inward-bulge type of buckle and evaluated the details of its shape mathematically using an energy approach. This resulted in equation (11), in which the buckle-shape parameter n appears. Through logical reasoning, using the known behavior of long, axially compressed, isotropic cylinders as a guide, Hoff constructed a chart in which $\sigma_c R/Et$, R/b, and n are related. This was done using the GALCIT data in conjunction with equation (11), which permitted the computation of n for each test specimen. The data were related by plotting R/b as ordinate and $\sigma_c R/Et$ as abscissa, with the value of n noted at each test point. Curves were then faired through the data. The resultant chart is shown in figure 7.

The early work at PIBAL consisted of tests of stiffened cylinders in bending for the purposes of evaluating general instability. The data from these tests were added to the chart used to relate the GALCIT cylinder parameters, after which the curves were refitted as shown in figure 7. It may be possible to use this chart as a check against further test data when n is known for a particular specimen. To use it for design or analysis, however, a prior knowledge of n is required. It is also possible to revise figure 7 with the aid of equation (11) so that n may be eliminated. Such a chart could be useful in design.

Physical Approach

It was mentioned in the section entitled "Review of Existing Data" that general instability in a stiffened circular cylinder consists of the inability of the circumferential frames to support the main load-carrying system of the cylinder. For bending loads the frames must provide radial restraint to the axial stiffeners in the compression region of the cylinder. The frame spacing must be small enough to preclude panel instability between frames, and the frame rigidity must be sufficiently great to support the stiffeners over an axial length roughly twice that at which the stiffeners would buckle as pinned columns under the loads induced in them by the external moment.

This frame stiffness criterion is employed in this section as the basis for computing the general instability stress of a stiffened circular cylinder in bending. This development is preceded by a review of the methods used previously to employ the frame rigidity criterion to evaluate bending general instability.

Frame spring constant.- In the earlier work done by GALCIT it was realized that the general instability of a stiffened circular cylinder could be related to the radial rigidity of the cylinder at a frame (refs. 7 and 8). This quantity P/δ, which was termed the "normal restraint coefficient," is the ratio of load to deflection when a concentrated radial force P is applied to the stiffened cylinder at any point on a frame and causes a radial deflection δ. It is actually the spring constant of the frame.

GALCIT devoted considerable study to this quantity. Dead weights were applied to the frame at center span at the extreme (lower) compression fiber of a test cylinder and radial deflection was measured as a function of bending moment. The curve of P as a function of δ was thus determined for the cylinder. It was found to be linear for bending moments up to three-fourths of those at general instability, after which the slope P/δ decayed rapidly until it appeared to vanish at general instability.

These results verified the hypothesis concerning the frame-spring-constant dependence of general instability in bending. GALCIT also found that the failure moment of a cylinder could be related to the normal-restraint coefficient for the unloaded cylinder. However, this relation required modification for the effect of the longitudinal spacing.

The theoretical approach developed by Hoff (ref. 30) and extended by PIBAL (refs. 15 to 18) yielded a parameter

$$\Lambda_o = \left(\frac{R}{d}\right)^4 \frac{I_s}{I_f} \tag{13}$$

which was suggested as an index to be used to evaluate bending general instability. According to PIBAL, if $\Lambda_o < 10$ general bending instability would not be expected; I_f and I_s are the distributed section moments of inertia in which effective sheet is omitted.

Shanley approached the problem of bending general instability by seeking a method to insure avoiding its occurrence (ref. 39). He extended the PIBAL concept by means of an approach similar to that used by GALCIT to derive normal-restraint coefficients. The result was a parameter embodying frame rigidity and loading

$$C_f = \frac{EI_fL}{MD^2} \tag{14}$$

Shanley plotted the GALCIT and PIBAL data in terms of this parameter as shown in figure 8 and selected the value of

$$C_f = \frac{1}{16,000} = 6.25 \times 10^{-5} \tag{15}$$

as a cutoff below which general instability may be expected and above which the likelihood is small.

Gerard obtained a similar result by considering the frame to be a transverse stiffener (ref. 27). In order to apply this analysis it was necessary to have an estimate of the shape of the buckle pattern of the cylinder in general instability. For this purpose the inward-bulge model was used with the PIBAL shape parameter n taken at its greatest value obtained from analysis of the GALCIT data. This value, 5.5, permitted calculation of C_f, for which Gerard found

$$C_f = 6.84 \times 10^{-5} \tag{16}$$

This value also is indicated in figure 8.

Calculation of general instability stress.- In this section the spring-supported stiffener-panel model of stiffened-cylinder behavior is used to derive a theoretical expression for the bending general instability stress. This approach parallels that of Gerard (ref. 27) in determining optimum design proportions of a stiffened cylinder, except for the form of the frame spring constant. This was obtained from data prepared by Wignot, Combs, and Ensrud (ref. 52) in which the frame is assumed supported by the sheet. The shearing rigidity of the sheet imparts restraint to the tangential-deformation tendency of the frame

thereby inducing into it a higher effective spring constant than it would theoretically have were it assumed to be supported according to the elementary theory of shear flow in cylinders.

The bending general instability stress is determined by assuming the cylinder structure near the extreme compression fiber to be a uniformly loaded, axially stiffened, rectangular curved plate supported by a system of transverse ribs acting as linear springs. The inward-bulge model is assumed to be as depicted in figure 2, which shows the plate width b to be the nodal distance on the profile of the inward bulge.

The buckling load of the critical stiffener is

$$P_{cr} = c\pi^2 \frac{E\bar{I}_s}{d^2} \tag{17}$$

It may be calculated utilizing the relation between stiffener end fixity and frame stiffness shown in figure 9, which was determined for flat stiffened plates by the method described in reference 5. As was shown in the section entitled "Strength of Stiffened Curved Plates," there is little influence of panel curvature on failure, and consequently it is permissible to utilize figure 9 in this analysis.

The end-fixity coefficient is equivalent to

$$c = \left(\frac{d}{L'}\right)^2 \tag{18}$$

and since

$$\sigma_c = \frac{P_{cr}}{A_s} \tag{19}$$

$$\left.\begin{aligned} A_s &= bt_s \\ \bar{I}_s &= bI_s \end{aligned}\right\} \tag{20}$$

the buckling stress is

$$\sigma_c = \frac{\pi^2 E\bar{I}_s}{A_s(L')^2} = \frac{\pi^2 EI_s}{t_s(L')^2} \tag{21}$$

The end fixity is related to the frame deflectional spring constant per inch of width of the panel K_f through the quantity

$$W = \frac{K_f d^3}{EI_s} \tag{22}$$

according to the curve of figure 9, when the axially stiffened plate is supported by an infinite number of transverse stiffeners. However, when four or more transverse stiffeners are present figure 9 may be used with little error. It should be noted that the transverse stiffeners are assumed to have bending rigidity only. The torsional rigidity in this case is zero.

This analysis is directed toward an expression for the bending general instability stress in terms of the equivalent panel width b' and the overall length of the buckle $2L'$. This latter quantity is the distance between effectively rigid frames in the cylinder and is one of the significant quantities in the data of Wignot, Combs, and Ensrud (ref. 52) relating to the frame spring properties.

It is possible to derive the following expression for W in which L' appears instead of d:

$$\overline{W} = \frac{K_f (L')^3}{EI_s} = \left(\frac{L'}{d}\right)^3 W \tag{23}$$

This may be plotted as a function of W, as shown in figure 10. It may be seen that

$$\overline{W} = 13.2 + 0.6W \tag{24}$$

is a close approximation to the curve in the region of general instability. By combining equations (23) and (24), it follows that

$$\overline{W} = \frac{13.2}{\left[1 - 0.6\left(\frac{d}{L'}\right)^3\right]} = \frac{K_f (L')^3}{EI_s} \tag{25}$$

The data of Wignot, Combs, and Ensrud lead to the following expression for the frame spring constant

$$\frac{P}{\delta} = \frac{RtG}{2L' c_\delta} \tag{26}$$

where

$$c_\delta = \frac{R^2}{4}\left(\frac{Gt}{EL'\bar{I}_f}\right)^{1/2} \tag{27}$$

The frame spring constant per inch of width K_f is $P/\delta b'$. Consequently, from equations (26) and (27),

$$K_f = \frac{2}{b'R}\left(\frac{tGE\bar{I}_f}{L'}\right)^{1/2} \tag{28}$$

When this expression is substituted into equation (23) and the relation $\bar{I}_f = I_f d$ is utilized, it is found that

$$\frac{EI_s}{(L')^2} = \frac{\dfrac{1 - 0.6\left(\dfrac{d}{L'}\right)^3}{6.6}(tGEI_fL'd)^{1/2}}{b'R} \tag{29}$$

When equation (21) is substituted into this expression, the buckling stress is found in the form

$$\sigma_c = \left\{\frac{\pi^2}{6.6}\left[1 - 0.6\left(\frac{d}{L'}\right)^3\right]\left(\frac{G}{E}\frac{L'd}{b'^2}\right)^{1/2}\right\}\frac{E(I_ft)^{1/2}}{Rt_s} \tag{30}$$

or

$$\sigma_c = \frac{gE}{Rt_s}(I_ft)^{1/2} \tag{31}$$

where

$$g = 1.5\left[1 - 0.6\left(\frac{d}{L'}\right)^3\right]\left(\frac{G}{E}\frac{L'd}{b'^2}\right)^{1/2} \tag{32}$$

The form of equation (31) differs from the result of Taylor (eq. (3)). The quantity g contains the geometric parameters of an inward bulge as depicted in figure 2. Consequently, the results of equation (31) could be compared with test results if data on buckle geometry were available. Unfortunately these data are not available.

Test Data

The test data obtained by both GALCIT and PIBAL on bending general instability of stiffened circular cylinders appear in figure 6. The data are plotted in the form of bending strain $\sigma/\eta E$ as a function of the GALCIT parameter

$$Q_b = \frac{(\rho_f \rho_s)^{3/4}(bd)^{-1/4}}{R} = \frac{t_e}{R} \tag{33}$$

in which $(\rho_f \rho_s)^{3/4}(bd)^{-1/4}$ is equivalent to an effective cylinder wall thickness t_e. The section properties are discussed subsequently.

The axial measured strains in the stiffness are shown plotted as a function of Q_b in figure 6. The GALCIT and PIBAL data on sheet-covered cylinders and the GALCIT data on wire-braced and unbraced specimens are included in this figure, from which it may be seen that the data on the sheet-covered and braced specimens may be fitted to linear curves throughout the entire stress range. The scatter in the GALCIT data for sheet-covered specimens is about 16 percent, while that of the PIBAL data is approximately 19 percent.

The linearity of the data permits the use of the following expression for the general instability stress in the same form as for moderate-length and long isotropic cylinders in axial compression or in bending:

$$\sigma_c = \frac{CEt}{R} \tag{34}$$

Utilizing the GALCIT parameter,

$$\sigma_c = 4.80EQ_b \tag{35}$$

for the GALCIT data on sheet-covered specimens, and

$$\sigma_c = 3.25EQ_b \tag{36}$$

for the PIBAL data.

The ratio of the GALCIT coefficient to the PIBAL coefficient is 4.80/3.25, or approximately 1.5. As discussed in the following section, the method of attachment of the frames, stiffeners, and sheet would be

expected to influence the effective value of J to be used in equation (3). In all cases the frames, stiffeners, and sheet were joined at their common intersection. However, the GALCIT frames were attached to the sheet in at least one additional position between stiffeners, while the PIBAL frames were attached to the sheet only at the stiffeners (fig. 11). In both cases the stiffeners were connected to the sheet at frequent intervals between frames. This difference in attachment would also be expected to decrease the effective sheet thickness.

It is interesting to note that the unbraced specimens apparently failed by Greenhill instability, in which the entire cylinder section at the midspan station rotates about the cylinder axis without deformation in its plane.

Section Properties

In the preceding discussions little mention was made of the effective section properties of the cylinder elements. Analysis of the test data and an evaluation of the behavior of a segment of the cylinder (presented below) reveal that the effective section properties would be essentially the geometric values except for the torsional rigidities of the stiffeners and frames. For the axial- and bending-section properties, effective sheet was included by GALCIT and PIBAL in calculating general instability stresses for comparison with test data.

The bending rigidities were computed by GALCIT (refs. 7 to 12) and PIBAL (refs. 16 and 18) utilizing various expressions for the effective sheet acting with these components of the cylinder structure. GALCIT found agreement of the test data with linear empirical theory when the full sheet width between frames was assumed to be effective, while the effective width found from

$$\frac{w_{e_s}}{b} = \frac{1}{3}\left(\frac{\sigma_{cr_c}}{\sigma_c}\right)^{1/3} \tag{37}$$

was used with the stiffeners. The geometric torsional moment of inertia was used for both the frames and stiffeners including effective sheet. The sheet rigidity was reduced to one-half of the nominal value to account for the buckled state of the sheet panels.

Calculations reveal that the large discrepancy between the Taylor theory and test data is little affected by changes in the assumed amounts of effective sheet acting with the stiffeners and frames. However, a large change in effective torsional rigidities of the stiffeners and frames would exert a strong influence upon theoretical buckling stresses.

This may be seen by examining the data shown in figure 6, which depicts the increase in bending general instability stress as the effective rigidity of the structure in the bays is increased.

If the frames, stiffeners, and sheet of a stiffened circular cylinder are closely spaced and rigidly connected to one another, then the maximum possible value of torsional rigidity of the cylinder wall can be realized. This is equal to the sum of the geometric section properties

$$\tilde{J} = J_s + J_f \tag{38}$$

in which the effective sheet widths are included.

However, the finite frame and stiffener spacings, and the flexible connections used on the test cylinders indicate that equation (38) is of dubious applicability for bending general instability. The minimum value of J is equal to that of the sheet alone. If Poisson's ratio is taken to be zero, then this value is

$$J = 2\,\frac{t^3}{6} = \frac{t^3}{3} \tag{39}$$

which is equivalent to $4\left(I_{sheet}\right)$.

On most of the GALCIT and PIBAL test specimens the geometric value of J_s exceeded that of J_f by a factor of 10 or more. In addition, the sheet-stiffener-frame connection consisted of only one aluminum rivet or steel screw in all cases (see fig. 11). From the standpoint of rigidity alone the principal structure for supporting internal torsion loads was the system of axial stiffeners, with which there could have been little interaction with the frame system.

The actual transmission of these loads required continuity which only the sheet could provide, since each stiffener would tend to twist independently of its adjacent stiffener. Some gain in effective rigidity of the sheet in twisting about a longitudinal axis might have been provided by the stiffeners on the test cylinders by means of the line of rivets used to connect them.

An increase in stiffener rigidity against twisting about a circumferential axis could be provided only by the frames, with suitable connections to the sheet. The data of figure 6 indicate the effect of the frame-sheet attachment.

Since the test-cylinder frame torsional rigidities were of the same order of magnitude as those of the sheet between frames, then the effective

torsional rigidity of the sheet-frame-stiffener system would depend upon the connection stiffnesses and the torsional rigidity of the frame and sheet. Thus it appears that J would be of the same order of magnitude as I_f for the low connection rigidity in the test cylinders.

The effective shear rigidity of the sheet was investigated experimentally by PIBAL by twisting stiffened circular cylinders which had been previously subjected to axial loads of various magnitudes (ref. 19). The result was a series of curves of effective shearing rigidity as a function of the ratio of applied axial strain to buckling axial strain. However, these data reveal appreciable scatter and appear also to be influenced by the method of attachment of the sheet to the stiffeners and frames. Since this is different in the PIBAL cylinders from that used in the GALCIT cylinders, another uncertainty is introduced. Evidently a method of evaluating the effective shearing rigidity of the sheet is required.

Discussion of Taylor's Theory

Taylor's theory involves the geometric and structural parameters of the cylinder as well as the geometric parameters of an assumed buckle shape in the orthotropic-cylinder solution to the axial-compression buckling problem. The assumed buckle shape is a continuous wave pattern which is sinusoidal both axially and circumferentially. This agrees with the solution assumed in the classical theory for the axial-compression buckling of unstiffened circular cylinders. Taylor's approach, then, is the basic mathematical solution to the problem of axial-compression buckling of an orthotropic circular cylinder, with the calculations simplified by use of the Donnell type equilibrium equation which he derived for orthotropic circular cylinders. Application of this axial solution to the problem of bending general instability is questionable. Furthermore, the large discrepancies between this theory and actual bending test data throw serious doubt upon the applicability of the method as it has been used in the past.

In the light of the preceding discussion on section properties, it is conceivable that the value of J used in past evaluations of Taylor's theory may have been too large. When the view is taken that J is of the order of I_f, then calculations show the possibility of obtaining agreement of Taylor's result with test data. This is now demonstrated.

It is possible to reduce Taylor's expression to a form similar to equation (31) by employing simplifications. Using $G/E = 1/2$ for $\nu = 0$, equation (3) becomes

$$\sigma_c = \frac{2E}{Rt_s}\left(\frac{\beta^2 I_f + \frac{J}{4}}{\frac{\beta^2}{t_s} + \frac{1}{t}}\right)^{1/2} \tag{40}$$

The quantity β is equal to the ratio of axial to circumferential wave lengths of the buckle L'/b'. Test data appear to indicate that $\beta > 1$.

If it is assumed that the first terms in the numerator and denominator in the parentheses of equation (40) predominate, then

$$\sigma_c = \frac{2E}{Rt_s}\left(I_f t_s\right)^{1/2} \tag{41}$$

Writing

$$t_s = \frac{g^2}{4}\,t \tag{42}$$

where g is a parameter whose value is yet to be determined, gives the equation

$$\sigma_c = \frac{gE}{Rt_s}\left(I_f t\right)^{1/2}$$

This equation is identical to equation (31), which was obtained on an entirely different basis. Using equation (32) or using $G/E = 1/2$ and $L'/b' = \beta$, together with the fact that $L'/d > 1$ for general instability, it may be permissible to simplify g to the form

$$g = 0.106\beta\left(\frac{d}{L'}\right)^{1/2} \tag{43}$$

or

$$g = 0.106\beta c^{1/4} \tag{44}$$

The parameter g may also be related to the expression for buckling stress obtained empirically. Equation (35) becomes, upon substitution of Q_b from equation (33),

$$\sigma_c = 4.80 \frac{E}{R}(\rho_s \rho_f)^{3/4}(bd)^{-1/4} \tag{45}$$

When σ_c from equations (31) and (45) are equated, it is found that

$$g = 4.80\left[\frac{b}{d}\frac{\rho_s}{\rho_f}\left(\frac{t_s}{t_f}\right)^2\left(\frac{t_s}{t}\right)^2\left(\frac{\rho_s}{b}\right)^2\right]^{1/4} \tag{46}$$

If equations (31) and (34) are equated, utilizing the expression for g from equation (46), then with t_s replacing t in equation (34),

$$C = 4.80 \frac{\rho_f}{t_s}\left(\frac{\rho_s}{b}\right)^{1/2}\left(\frac{b}{d}\frac{\rho_s}{\rho_f}\right)^{1/4} \tag{47}$$

in which R is absent.

These results unite Taylor's theory with the physical approach and the test data.

Effect of Plasticity

The GALCIT data shown in figure 6 are substantially linear to a maximum strain of 0.0062 inch per inch. These tests were performed on 2017-T4 aluminum-alloy sheet and tubing for which the proportional limit is approximately 30,000 psi and the yield stress is roughly 40,000 psi. For this material the maximum measured test strain of 0.0062 corresponds approximately to the yield strength and consequently is well into the inelastic range.

The linearity of the GALCIT data in the plot of longitudinal failure strain as a function of Q_b suggests the use of the secant modulus as the pertinent plasticity-reduction factor for orthotropic cylinders in bending. For any other plasticity-reduction factor, strain would be functionally related to Q_b in some manner other than linear.

OPTIMUM DESIGN FOR BENDING

General Background

The problem of designing a structure for minimum weight has received considerable attention in recent years. It has been demonstrated by several investigators that a composite structure subject to instability can have a weight that is a mathematical minimum. This is in contrast to a tension loaded structure, the least weight of which is determined by the ultimate tensile strength of the construction material.

This section contains data on minimum weights for stiffened circular cylinders in bending. The approach essentially follows the fundamental mathematical procedure employed by Gerard (ref. 27). This work should be consulted for a thorough treatment of the subject of minimum-weight analysis. This report contains an outline of the method of analysis and a summary of the results.

Basic Concepts of Minimum-Weight Analysis

The fundamental concepts of minimum-weight analysis are:

(1) All possible buckling or failure modes occur simultaneously. This is virtually an axiom in minimum-weight analysis which is usually accepted without proof. Recently, however, Gerard presented a demonstration of this concept. The obvious result of this axiom is the equality of the buckling stresses of the various modes.

(2) There is no interaction between buckling modes. Data tend to substantiate this for an optimum structure. Simultaneous buckling of all modes without interaction is equivalent to failure of the component.

(3) The fundamental unit is solidity, which is the ratio of structural volume inside a surface to the total volume enclosed by the surface. In minimum-weight analysis the solidity is determined in terms of the parameters of the problem. Minimization of solidity with respect to the variable parameters provides the equations which lead to the proportions yielding minimum weight.

(4) The variable parameters are usually lengths. In a typical design problem certain "closed" parameters are selected from nonstructural considerations, such as fuselage diameter, wing contour, spar location, and so forth. The "open" parameters may be fuselage frame size and spacing, wing cover proportions, and the like. In addition, the external forces on these structures are known.

As a result the loading on a given structure is known and the minimum-weight analysis consists of determining the dimensions of the open parameters which will lead to the lightest weight structure that is capable of resisting the applied loading at incipient buckling.

Stiffened Circular Cylinders in Bending

For the analysis of this case the section selected for solidity determination is that of the cylinder between a pair of adjacent frames. Then

$$\Sigma = \frac{2\pi R t_s d + 2\pi R t_f d}{\pi R^2 d} \tag{48}$$

where t_s contains the full width of sheet between stiffeners and $t_f d$ $(=A_f)$ includes the frame cross-section area alone.

As shown in Part V of the Handbook (ref. 5), the effective distributed stiffener area is obtained from axially loaded optimum stiffened-panel data as

$$t_s = \left(\frac{N_x d}{\alpha_p{}^2 c^2 \bar{\tau} E} \right)^{1/2} \tag{49}$$

which contains the structural efficiency parameter α_p, the end-fixity coefficient c, and the generalized plasticity-reduction factor $\bar{\tau}$. The loading N_x is determined in the usual manner from the applied moment and cylinder section modulus.

The frame area is obtained from the frame stiffness criterion for general instability as follows:

$$A_f = \frac{\pi R^2 C_f N_x}{E \rho_f{}^2 d} \tag{50}$$

in which C_f is the minimum value of the frame stiffness coefficient as discussed in the section entitled "Bending General Instability." The frame radius of gyration ρ_f does not include any effective sheet.

When equations (49) and (50) are substituted into equation (48), which is then minimized, it is found that the minimum-weight conditions for a stiffened cylinder constructed of one material are as follows:

(a) The frame weight should be one-fourth of the sheet-stiffener-panel weight.

(b) In the elastic range the optimum cover thickness is given by

$$\left(\frac{t_s}{R}\right)_o = \frac{4C_f}{\alpha_p^3}\left(\frac{\pi c^{1/2} M}{R^2 E d}\right)^{1/2} \frac{R}{\rho_f} \tag{51}$$

and the optimum frame spacing is

$$\left(\frac{d}{R}\right)_o = \left(16\pi C_f \alpha_p c^{1/4}\right)^{2/5}\left(\frac{R}{\rho_f}\right)^{4/5}\left(\frac{M}{\pi E R^3}\right)^{1/5} \tag{52}$$

The optimum solidity is shown in figure 12 as a function of applied bending moment with the data corrected for the centroidal distance of the stiffener from the surface of the shell. Curves are shown on the figure for Y-stiffened panels, for which $\alpha_p = 1.15$. This graph also contains data for the optimum unstiffened circular cylinder and for the hypothetical shell of minimum weight for which the optimum stress $\sigma_{cy} = 69{,}000$ psi (7075-T6 aluminum alloy).

CUTOUT CYLINDERS IN BENDING

Introduction

The general instability of stiffened circular cylinders with cutouts was investigated by PIBAL (refs. 20 to 25). Bending tests were performed on cylinders with symmetric cutouts and with side cutouts, and theoretical analyses were performed using the energy approach.

Test Data

The symmetric cutouts were located at the extreme compression fibers of the cylinders, while the side cutouts were at the centroidal axes of the cylinder cross sections on one side only. Figures 13 and 14 depict these specimens schematically. It should be noted that the stiffeners framing the cutouts were the same as those in the remainder of the cylinder. Longerons were not used at the edges of the cutouts. The symmetric-cutout specimens had the same cross-section properties and all cutouts were the same length. Two overall cylinder lengths were used, and the cutout angles were 45°, 90°, and 135°.

The side-cutout specimens differed in virtually all respects. The number of stiffeners, length of cutout, length of cylinder, and angle of cutout were all varied.

The results of the tests on the cutout cylinders appear in figures 13 and 14 in which general instability bending moment is plotted as a function of cutout angle. For symmetrical cutouts there appears to be a strong influence of cutout angle upon general instability, whereas for the side-cutout cylinders the influence appears to be small when the cutout angle θ exceeds 90°.

It was observed at PIBAL that although general instability was the principal buckling mode in all cases, collapse occurred at this stress level only in the symmetrical-cutout specimens and not in those with side cutouts. The latter sustained bending moments after general instability which occurred at the compression side of the cutout. However, a sudden decrease of load followed general instability and succeeding bending moments at further deformation never exceeded those at which instability first occurred. As many as three successive load rises and drops were observed as the bending curvature increased, which corresponded to additional buckling of stiffeners after the occurrence of general instability at the cutout.

Theory

Before PIBAL computed the general instability stress of a stiffened cylinder it was necessary to know the stress field before buckling. For a cylinder without cutouts this is a relatively simple problem. For one with cutouts, however, a rather complex analysis is required. PIBAL utilized a numerical procedure for this purpose, and strain measurements made on the test specimens before buckling revealed good agreement with this theory.

The buckling analysis was performed utilizing strain energy. The energy of the structure in the buckled form was computed for radial bending, circumferential bending and torsion in the stiffeners (including effective sheet), bending of the frames in their planes, and shear in the sheet in the buckled state. The buckle waveform was represented by a sine curve extending the length of the cutout and by the first seven terms of a Fourier series in the circumferential direction. The coefficients were determined from boundary conditions and by minimization to obtain the buckling loading.

An empirical procedure for analysis may be devised from the observed behavior of uncut stiffened circular cylinders, utilizing the concepts relevant to the frame stiffness criterion presented in the section on the physical theory of bending general instability. This employs the hypothesis that the circumferential extent of the inward bulge is small compared with the periphery of the cylinder, and consequently the axial compression stresses in this region are virtually constant. The effective frame in this area acts as a deflectional spring to support the axial stiffening system.

As a result of this assumption, the bending general instability stress of a symmetric cutout cylinder would be the same as that at the extreme fiber of a complete cylinder. A test of this hypothesis would be a comparison of buckle waveforms of the cut and whole cylinders. However, such data are unavailable.

On the basis of this approach, the bending strength of a stiffened cylinder with a symmetric cutout would be directly proportional to the section modulus of the cylinder cross section. An analysis based upon this hypothesis appears in the following section.

Effective Section Modulus of Symmetric-Cutout Cylinder in Bending

It is assumed, in the following derivation, that the effective thickness of the cylinder wall is constant, although there actually may be a loss of sheet effectiveness on the compression side.

The geometry of the cutout cylinder is shown in figure 13, to which the following equations apply:

$$A = 2tR \tag{53}$$

$$\bar{y} = \frac{\int_0^{\alpha} (R \cos \phi) tR \, d\phi}{\int_0^{\alpha} tR \, d\phi} = \frac{R \sin \alpha}{\alpha} \tag{54}$$

$$I_{xx} = 2\int_0^{\alpha} (R \cos \phi)^2 tR \, d\phi = tR^3(\alpha + \sin \alpha \cos \alpha) \tag{55}$$

$$I_{NA} = I_{xx} - A\bar{y}^2 = tR^3\left(\alpha + \sin \alpha \cos \alpha - \frac{2 \sin^2 \alpha}{\alpha}\right) \tag{56}$$

The extreme fiber distance to the compression edge is

$$e = R\left(\frac{\sin \alpha}{\alpha} - \cos \alpha\right) \tag{57}$$

The section modulus for the compression fiber is then

$$Z = \frac{I_{NA}}{e} = R^2 t \, \frac{\alpha + \sin \alpha \cos \alpha - \frac{2 \sin^2 \alpha}{\alpha}}{\frac{\sin \alpha}{\alpha} - \cos \alpha} \tag{58}$$

For the complete cylinder

$$Z_o = \pi R^2 t \tag{59}$$

and, consequently,

$$\frac{M}{M_o} = \frac{Z}{Z_o} = \frac{\alpha + \sin\alpha\cos\alpha - \frac{2\sin^2\alpha}{\alpha}}{\pi\left(\frac{\sin\alpha}{\alpha} - \cos\alpha\right)} \tag{60}$$

In terms of the cutout angle θ,

$$\alpha = \pi - \frac{\theta}{2} \tag{61}$$

and, consequently, equation (60) becomes

$$\frac{M}{M_o} = \frac{\left(\pi - \frac{\theta}{2}\right) - \frac{1}{2}\sin\theta - \frac{1 - \cos\theta}{\pi - \frac{\theta}{2}}}{\pi\left\{\left[\frac{\left(\frac{1 - \cos\theta}{2}\right)^{1/2}}{\pi - \frac{\theta}{2}}\right] + \cos\frac{\theta}{2}\right\}} \tag{62}$$

Comparison of Theory and Test Data

The test data and theory are compared in figures 13 and 14. There is little noticeable scatter in the data for the symmetric-cutout cylinders, and the two sets of test points (for 8 stiffeners and 16 stiffeners) appear to define smooth curves for the side-cutout cylinders. The theoretical and experimental trends of critical moment as a function of cutout angle seem to agree for the symmetric cutouts, although the PIBAL theory predicts instability stresses which average about 35 percent greater than the test data.

The fabrication details of one of the uncut cylinders tested in the earlier PIBAL series correspond to those of the symmetric-cutout cylinders. This permits determination of the reduction in strength as the result of a cutout for this cylinder. With $M_o = 290{,}000$ inch-pounds at $\theta = 0$ for the data in figure 13, the curve of M as a function of the cutout angle θ appears as shown. The curve of M as a function of θ, derived using equation (62), is presented for comparison. The agreement is seen to be good.

The discrepancy between theory and experiment is quite marked for the side-cutout cylinders. Both the magnitude and trend of moment as a function of cutout angle differ in this case. An attempt to apply the section-modulus method to this case failed. Part of the difficulty may lie in the steep stress gradients that exist near the cutout edges when θ is small. Also, the principal axes of the cutout cylinder would be rotated away from the plane of symmetry through the cutout as a result of the loss of sheet effectiveness on the compression side of the cylinder.

PRESSURE GENERAL INSTABILITY

Introduction

General instability of longitudinally stiffened circular cylinders under inward pressure is one of the few fields of interest in which no test data appear to have been published. Thus the available data are exclusively theoretical.

Timoshenko (ref. 53) has discussed general results obtained from the solution of Flügge's three differential equations for orthotropic cylinders (ref. 32) applied to the case of external pressure loading. Energy solutions to this problem were advanced by Salerno and Levine (ref. 41), Kendrick (ref. 42), and Nash (ref. 54) for ring-stiffened cylinders. For this same case Bodner employed energy methods to derive a Donnell type partial differential equation (ref. 40) for orthotropic cylinders similar to equation (2), which he applied to this problem.

Becker (ref. 43) employed the approach of Taylor, which includes the assumption that $\nu = 0$, to derive the extended form of the Donnell type orthotropic-cylinder equation presented in this report as equation (2). This equation was used to obtain an explicit relation between general instability stress and the geometric parameters of a moderate-length circular cylinder stiffened both axially and circumferentially and loaded by external pressure.

In all these cases the cylinder ends were assumed to be simply supported and calculations were restricted to the elastic range. These theories are presented in this section in which attention has been focussed upon moderate-length and long cylinders. A discussion is included on effective section properties for stiffened cylinders loaded by external pressure.

Moderate-Length Cylinders

The general instability stress for moderate-length stiffened circular cylinders under inward radial or hydrostatic pressure is

$$\sigma_y = 5.51E\left(\frac{t_s}{t_f}\right)^{1/4}\left(\frac{\rho_f}{R}\right)^{3/2}\left(\frac{R}{L}\right) \tag{63}$$

This result is obtained on the assumption that the ratio of the circumferential wave length of the buckle to the longitudinal wave length is negligible compared with unity. This assumption facilitates obtaining the

explicit form of the general instability stress shown in equation (63). The circumferential compressive stress applied to the cylinder is

$$\sigma_y = \frac{pR}{t_f} \tag{64}$$

Bodner (ref. 40) has analyzed the general instability of ring-stiffened cylinders under hydrostatic pressure employing the Donnell type orthotropic cylinder differential equation in which $\nu \neq 0$. The results are depicted in the chart of k_p as a function of Z_L (fig. 15) where

$$k_p = \frac{12(1 - \nu^2)pRL^2}{\pi^2 E t^3} \tag{65}$$

and

$$Z_L = \frac{L^2}{Rt}(1 - \nu^2)^{1/2} \tag{66}$$

This chart corresponds to those presented in Part III (ref. 3) for all types of cylinder behavior. It depicts the length spectrum from flat-plate action through moderate-length-cylinder behavior.

For ring-stiffened-cylinder construction under radial pressure,

$$t_s = t \tag{67}$$

$$\sigma_y = \frac{pR}{t_f} \tag{68}$$

Then, using $\nu = 0$, which applies to equation (63), equation (65) becomes

$$k_p = 6.70\left(\frac{t_f}{t}\right)^{3/4}\left(\frac{\rho_f}{R}\right)^{3/2} Z_L \tag{69}$$

Bodner (ref. 40) employed a parameter which, for moderate-length cylinders with the frame centroids at the shell surface, is

$$F = \frac{12(1 - \nu^2)I_f}{t^3} - 1 \tag{70}$$

in which I_f does not include effective sheet.

An expression for F relating to frames with centroids removed from the shell surface, and including effective sheet, appears subsequently with the data on section properties.

Since $I_f = \rho_f^2 t_f$, then equation (70) becomes

$$F = 12(1 - \nu^2)\left(\frac{t_f}{t}\right)\left(\frac{\rho_f}{t}\right)^2 - 1 \tag{71}$$

For large values of $\left(\frac{t_f}{t}\right)\left(\frac{\rho_f}{t}\right)^2$ and $\nu = 0$,

$$F = 12\left(\frac{t_f}{t}\right)\left(\frac{\rho_f}{t}\right)^2 \tag{72}$$

and equation (69) becomes

$$k_p = 1.04F^{3/4}Z_L^{1/2} \tag{73}$$

Equation (73) yields stresses which lie less than 10 percent below those obtained from Bodner's curves for $Z_L = 100$.

For moderate-length isotropic cylinders equation (63) agrees closely with the following result obtained by Batdorf:

$$\sigma_y = 0.93E\left(\frac{t}{R}\right)^{3/2}\frac{R}{L} \qquad \left(100\,\frac{t}{R} < \left(\frac{L}{R}\right)^2 < \frac{5R}{t}\right) \tag{74}$$

utilizing $\rho^2 = t^2/12$. Differences in the values of the constant are due to Poisson's ratio. The general instability stress for moderate-length cylinders is virtually the same for external radial and hydrostatic pressure loadings, and consequently equations (63) and (73) are applicable to both these conditions for $Z_L \geq 100$.

Bodner compared his results with an analysis based upon Flügge's three orthotropic cylinder equations (the results of which are discussed by Timoshenko, ref. 53) and with the calculations of Kendrick (ref. 42). Presumably the omissions in the theory of Salerno and Levine (ref. 41) render it of questionable utility, since it was not included in the comparison. The comparison was made on five cylinder designs for all of which $Z_L = 2{,}000$ and $0 < F < 20$. In general, the predicted stresses

cover a range of roughly 15 percent about the average value with Bodner's method highest and Kendrick's lowest. This would place equation (73) slightly above the average.

Long Cylinders

The general instability stress for a long stiffened cylinder under external pressure is

$$\sigma_y = 3E\left(\frac{\rho_f}{R}\right)^2 \tag{75}$$

which follows directly from the result of Levy (ref. 55) for the buckling of rings under inward radial load.

When this expression is substituted into equation (64) utilizing equations (65) through (68),

$$k_y = k_p = \frac{0.30FZ_L}{\frac{R}{t_f}} \tag{76}$$

where

$$F = 12\,\frac{t_f}{t}\left(\frac{\rho_f}{t}\right)^2 \qquad (\nu = 0) \tag{77}$$

For isotropic cylinders, $F = t_f/t = 1$ and

$$k_y = k_p = \frac{0.3Z_L}{\frac{R}{t}} \qquad (\nu = 0) \tag{78}$$

which agrees with the curves shown in Part III.

Section Properties

Nominal section properties were employed in deriving the buckling-stress expressions presented in this section. The stiffener and frame torsional rigidities and the sheet shear rigidity are absent from these expressions, and consequently only the selection of stiffener and frame effective sheet for area and bending moment of inertia is necessary.

As indicated in the preceding explicit expressions for external pressure general instability stress, the frame radius of gyration apparently exerts the greatest influence. This is evident in equation (63) in which it appears to the 3/2 power, and in equation (75) in which it is squared. Since the frame is subjected to normal loading in this case, the effective sheet acting with the frame will influence the effective value of ρ_f and, consequently, should be taken into account. This may be done using

$$\frac{w_{e_f}}{d} = 0.5\left(\frac{\sigma_{cr_y}}{\sigma_y}\right)^{1/2} \tag{79}$$

which is a commonly used relation for finding effective width of compressed plates.

The effective sheet acting with the axial stiffeners might be assumed to be the full width between stiffeners for radial pressure only, in analogy with the treatment of the frame effective width for bending as done by GALCIT. However, σ_y is proportional to $(t_f)^{1/4}$, and consequently differences in the amount of effective sheet acting with the axial stiffeners would be minimized by the 1/4-power exponent. Furthermore, in actual applications it is probable that hydrostatic loading will be encountered. Consequently, it would appear reasonable to find the axial stiffener effective sheet from

$$\frac{w_{e_s}}{b} = 0.5\left(\frac{\sigma_{cr_y}}{\sigma_y}\right)^{1/2} \tag{80}$$

Bodner (ref. 40) and Kendrick (ref. 42) presented methods for determining effective sheet acting with the frames of cylinders without axial stiffening. The result is essentially equivalent to the results obtained by using equation (79).

Bodner presented an expression for the frame parameter F which includes the effect of eccentricity of the frame from the center of the sheet as follows:

$$F = \frac{12(1 - \nu^2)\left[I_f + t_f(e - \bar{z})^2\right]}{t^3} + \frac{2w_{e_f}}{d}\left(1 + \frac{12\bar{z}^2}{t^2}\right) - 1 \tag{81}$$

By utilizing equation (79), this becomes

$$F = \frac{12(1 - \nu^2)\left[I_f + t_f(e - \bar{z})^2\right]}{t^3} + \left(\frac{\sigma_{cr_y}}{\sigma_y}\right)^{1/2}\left(1 + \frac{12\bar{z}^2}{t^2}\right) - 1 \quad (82)$$

which reduces to equation (70) when e and $\bar{z}$ vanish, provided that $\sigma_y \leqq \sigma_{cr_y}$. When $\sigma_y \geqq \sigma_{cr_y}$,

$$F = \frac{12(1 - \nu^2)I_f}{t^2} + \left(\frac{\sigma_{cr_y}}{\sigma_y}\right)^{1/2} - 1 \quad (83)$$

It should be noted that I_f, as used by Bodner, does not contain effective sheet. This is embodied in the stress-ratio terms in equations (82) and (83).

The buckling-stress expressions presented in equations (63) and (75) were derived on the basis of nominal section properties. The effective-width relations shown in equations (79) and (80) may be used with these equations.

TORSION GENERAL INSTABILITY

Introduction

Investigation of stiffened circular cylinders in torsion was initiated with the GALCIT test program (refs. 12 and 13). The buckling stress was plotted as a function of a parameter, similar to that for bending, which GALCIT derived on the basis of empirical reasoning (ref. 13).

A theory for torsional general instability was developed by Hayashi (ref. 45) utilizing an orthotropic Donnell equation similar to equation (2). Hayashi demonstrated that the parameters employed by Donnell to relate the geometric properties and loading of an isotropic cylinder (ref. 38) could be generalized to include the effects of orthotropicity. When this is done, the behavior of isotropic cylinders in torsion becomes a special case. The curves derived by Donnell may be used for orthotropic cylinders by using the generalized parameters in place of the isotropic parameters. Hayashi's treatment, therefore, covers the entire length range.

The theoretical results obtained by Hayashi are in implicit form. In order to determine plasticity-reduction factors, to evaluate optimum design under torsion loads, and to provide a simple relation between loading and general instability stress, it is desirable to utilize an explicit form of the instability stress relation. This was done in reference 43 for moderate-length and long cylinders.

In the following discussions theory and test data are described and compared.

Theory

GALCIT employed an empirical approach for cylinders in torsion comparable to that employed for cylinders in bending. This procedure led to the derivation of a parameter

$$Q_t = \left(\rho_f \rho_s\right)^{7/8} (bd)^{-1/2} (R)^{-3/4} \tag{84}$$

which was selected as the independent variable. Correlation was sought in terms of a relationship in the form

$$\frac{\tau}{E} = C Q_t \tag{85}$$

Hayashi analyzed stiffened cylinders in torsion using a form of the orthotropic Donnell equation similar to equation (2) except for the inclusion of Poisson's ratio. The mathematical solution utilizes the generalized form of the parameters to be used on the curve of k_s as a function of Z_L, which has been reproduced in figure 16. This curve was first obtained by Donnell (ref. 28) and later was revised by Batdorf, Stein, and Schildcrout (ref. 56).

The values of k_t and Z_L are given as follows for short and moderate-length orthotropic cylinders fabricated from one material:

$$k_t = \frac{\tau t L^2}{\pi^2 E I_f}\left(1 - \nu_{xy}\nu_{yx}\right) \tag{86}$$

$$Z_L = \frac{L^2}{2R}\left(1 - \nu_{xy}\nu_{yx}\right)^{1/2}\left(\frac{t_s}{3I_f}\right)^{1/2} \tag{87}$$

where ν_{xy} and ν_{yx} are the orthotropic Poisson's ratios.

For the isotropic case these reduce to the parameters

$$k_t = \frac{12\tau L^2}{\pi^2 E t^2}(1 - \nu^2) \tag{88}$$

$$Z_L = \frac{L^2}{Rt}(1 - \nu^2)^{1/2} \tag{89}$$

shown on the corresponding curve in Part III.

The theoretical result derived in reference 43 and shown in table 1 for general instability of moderate-length orthotropic circular cylinders loaded in torsion is

$$\tau = 3.46E\left(\frac{t_s}{t}\right)^{3/8}\left(\frac{I_f}{R^2 t}\right)^{5/8}\left(\frac{R}{L}\right)^{1/2} \tag{90}$$

for $\nu_{xy} = \nu_{yx} = 0$.

Equation (90) may be written

$$\frac{\tau}{E} = 3.46Q_t' \tag{91}$$

where

$$Q_t' = \left(\frac{t_s}{t}\right)^{3/8}\left(\frac{I_f}{R^2 t}\right)^{5/8}\left(\frac{R}{L}\right)^{1/2} \tag{92}$$

Since all the GALCIT test specimens were fabricated with R/L equal to 1/4, then for comparison with the test data it is possible to relate shearing stress to the section properties of the cylinders in the form

$$\tau = 1.73\bar{Q}_t = 1.73\left(\frac{t_s}{t}\right)^{3/8}\left(\frac{I_f}{R^2 t}\right)^{5/8} \tag{93}$$

For long cylinders Hayashi obtained

$$\tau = 1.754\left(1 - \nu_{xy}\nu_{yx}\right)^{-3/4}\left(\frac{t_s}{t}\right)^{1/4}\left(\frac{I_f}{R^2 t}\right)^{3/4} \tag{94}$$

which reduces to Donnell's result for isotropic cylinders and which agrees with the expression in reference 43 for $\nu_{xy} = \nu_{yx} = 0$.

Section Properties

Section properties for the cylinders loaded in torsion were determined by GALCIT on the basis of the best fit to the linear curve which was sought, as described below. This fit was obtained when the sheet was assumed to be fully effective in computing the stiffener and frame cross-section moments of inertia.

The correlation between the mathematical theory and the test data yielded best agreement when the effective widths of the sheet were determined utilizing the relations

$$\frac{w_{e_s}}{b} = 0.5\left(\frac{\tau_{cr}}{\tau}\right)^{1/2} \tag{95}$$

$$\frac{w_{e_f}}{d} = 0.5\left(\frac{\tau_{cr}}{\tau}\right)^{1/2} \tag{96}$$

Test Data

The test data obtained by GALCIT pertain exclusively to moderate-length cylinders. Observation of the behavior of the test specimens revealed that in many cases buckling began in a small region of the cylinder and gradually extended over the entire cylinder as the load was increased. Some of the cylinders supported twice the initial buckling stress before failure. The data reported herein, however, are confined to failure. This information is tabulated in reference 13.

The highest failure shear stress recorded in the GALCIT tests was 19,200 psi. A strong tension field existed in this specimen at failure, and, consequently, the equivalent axial tension stress in the sheet was approximately 38,000 psi. This corresponded to the proportional limit of the sheet covering of this particular specimen, as obtained from stress-strain curves. Stress-strain data for the stiffeners, frames, and sheet revealed a proportional limit between 40 and 50 ksi for the sheet and between 30 and 40 ksi for the frames. Consequently, it would appear that the effects of plasticity on the general instability stress were slight.

Comparison of Theory and Test Data

When shearing stress is plotted as a function of Q_t, as shown in figure 17, it is found that

$$\frac{\tau}{E} = 0.56(Q_t)^{0.80} \tag{97}$$

which is different from the form of equation (85). The data scatter about equation (97) is approximately 30 percent throughout the entire stress range.

The curve obtained using equation (93) is compared with the test data in figure 18, which reveals agreement within a scatter of about 30 percent up to a stress level slightly greater than 10 ksi. The average curve through the data is 5 percent below theory. These results are comparable to those obtained from torsion tests on isotropic cylinders, reported in Part III, in which the data scatter between theory and 40 percent below, with an average 16 percent below.

The dropoff in the data below the average curve at stresses above 10 ksi appears to be related to tension-field action. Insufficient data are available to evaluate this effect. Furthermore, at torsional shearing stresses approaching the upper limit of the data the effects of plasticity begin to enter the picture.

TRANSVERSE-SHEAR GENERAL INSTABILITY

Introduction

A theoretical analysis of transverse-shear general instability has not been published. However, it appears likely that the result for torsion loading may be employed for shear loading with suitable modification. An appropriate factor utilizing the GALCIT data on cantilevered cylinders and on cylinders loaded in torsion is presented as follows.

Modification to Torsion Data

GALCIT tested cylinders in combined bending and transverse shear (ref. 11) and reported that failure occurred either in a bending mode or a shear mode. There did not appear to be any interaction. This makes it possible to evaluate general instability in shear by comparing these test data with those for torsion on corresponding cylinders.

Four GALCIT moderate-length cylinders were reported to have failed in shear. For these cylinders the shear stress at failure was computed from

$$\tau_v = \frac{V}{\pi R t} \tag{98}$$

This stress was compared with the corresponding torsional failure stress determined from

$$\tau_t = \frac{T}{2\pi R^2 t} \tag{99}$$

It was found that $0.98 > \frac{\tau_v}{\tau_t} > 0.85$, with an average value at 0.92. These ratios are considerably lower than the value of 1.6 reported for isotropic cylinders in Part III.

Apparently it is possible to calculate transverse shear general instability in moderate-length stiffened cylinders utilizing equation (90), with a conservative 15-percent reduction as indicated above as follows:

$$\tau = 2.94E\left(\frac{t_s}{t}\right)^{3/8}\left(\frac{I_f}{R^2 t}\right)^{5/8}\left(\frac{R}{L}\right)^{1/2} \tag{100}$$

The need for the reduction factor is uncertain in view of the 30-percent scatter in the torsion data and the small number of transverse-shear test specimens. In the absence of more reliable data, the conservative expression, equation (100), could be used instead of equation (90).

COMBINED BENDING AND TORSION GENERAL INSTABILITY

Introduction

Information on general instability of stiffened circular cylinders under combined bending and torsion is limited to experimental data obtained by GALCIT (ref. 12). By means of these data it is possible to derive an interaction equation for this load combination. The data and the resulting equation are discussed as follows.

Interaction Equation

Structural interaction has been observed between the torsional and bending buckle patterns when these two loadings are applied simultaneously to a stiffened circular cylinder. For an isotropic cylinder, the pertinent interaction equation was shown to be (ref. 3)

$$\frac{\sigma}{\sigma_o} + \left(\frac{\tau}{\tau_o}\right)^2 = 1 \tag{101}$$

When GALCIT applied this relation to the test data considerable scatter was found. The test points lay between the parabolic curve of equation (101) and the circular curve

$$\left(\frac{\sigma}{\sigma_o}\right)^2 + \left(\frac{\tau}{\tau_o}\right)^2 = 1 \tag{102}$$

Because of this scatter and the difficulty of obtaining consistent data on the buckled cylinders as a result of the variations in buckle pattern, the test data are plotted in figure 19 in the form of T/T_o as a function of M/M_o. The test data agree fairly well with the parabolic interaction equation

$$\frac{M}{M_o} + \left(\frac{T}{T_o}\right)^2 = 1 \tag{103}$$

The separate loadings M_o and T_o were obtained directly from test data, as were the loads M and T which were applied simultaneously. For design purposes the separate loadings may be obtained from the general instability stresses which may be found in the sections entitled "Bending General Instability" and "Torsion General Instability," together with the appropriate section properties of the cylinder. When the permissible combination of applied loads is found, the individual general instability stresses may be found by reversing this process.

REVIEW OF STATE OF THE ART

At this point it appears worthwile to review the state of the art in the light of the data presented in this report.

The sparse data available on buckling of stiffened curved plates show an apparent decrease of buckling stress with curvature, which is contrary to expectations. However, considerably more test data would be required in this area before general conclusions should be drawn.

As a result of the data presented in the previous sections, theory and data for bending and torsional general instability of stiffened cylinders have been brought into agreement. In addition, the correlation between theory and test data for these two cases and the general agreement of the results of the differential-equation solutions with those based upon energy methods for external pressure loadings indicate that a mathematical approach to the problem of general instability is sound.

As was demonstrated herein, a useful tool for this purpose is the orthotropic differential equation which corresponds to that derived by Donnell for isotropic cylinders. It was applied successfully to bending, external pressure, and torsional loadings and should be useful for other problems in general instability. In fact, it is reasonable to assume that this type of equation provides a unified approach to the solution of such problems.

Of particular interst is the result of the investigation of bending general instability. It is evident, from the data presented in figure 6, that the rigidity of the shear-carrying structure in the cylinder panels has a strong influence upon the bending strength of a specific axial and circumferential stiffener configuration. The data appear to lend credence to the suggestion that the applicability of Taylor's theory depends strongly upon the choice of J. This theory would be useful in design and analysis if some prior method were available to determine g so that equation (31) could be applied without requiring a knowledge of the buckle dimensions.

The significance in the choice of J is emphasized by the gradual trend toward higher instability stresses as the shear-structure rigidity increases. A particularly significant point appears to be the ratio of the GALCIT test stresses to the PIBAL stresses with the principal difference between the two types of test specimens being the sheet-frame attachment.

The cylinders tested by GALCIT and PIBAL may be classified as built-up orthotropic, in which the element attachments influence the general instability stress. The effect of attachments would be eliminated in a monolithic orthotropic structure, and if it were possible to derive a relation between $\sigma_c/\eta E$ and Q_b for this case, it might be expected to provide an upper limit for the curves in figure 6. Another limiting case would be the isotropic cylinder, in which the shear-carrying structure

and the stiffener systems merge. Thus, two problems remain for bending general instability. One involves determining the monolithic-cylinder behavior and relating instability stress for built-up construction to that for monolithic construction as a function of shear-carrying structure and attachment rigidity. The second requires defining the transition from monolithic stiffened construction to isotropic construction.

In connection with bending general instability, it is of interest to note that the expressions derived by the Taylor and physical theories reduce to the modified classical form

$$\sigma_c = \frac{CEt}{R} \tag{104}$$

whereas Hoff's theory and the GALCIT empirical expressions do not lead to such a result.

An examination of equations (63) and (75) for external pressure loads indicates that the general instability stress for this case should be relatively insensitive to the behavior of the shear-carrying structure and its interaction with the stiffening system.

The influence upon torsional general instability stresses of the shear-carrying structure in the cylinder panels may be small. In this case the sheet is the principal load-carrying material, and, consequently, interaction with the axial and circumferential stiffeners does not appear to be important, as might be inferred from equations (90) and (91). These expressions were derived directly without assumptions as to the effective section properties.

In summary, it appears that only in the case of bending instability is the type of frame-sheet connection important, and the effective torsional rigidity differs significantly from the geometric section property. Effectively, then, many of the points raised in the previous summary of the state of the art have been resolved, for the most part, with the exception of the amount of nonlinearity in bending general instability and the predictive accuracy of the theories for external pressure on stiffened cylinders.

The future work in this field should emphasize testing to permit more reliable evaluation of the theories for curved stiffened panels in compression and for stiffened cylinders in bending and under external pressure. The absence of these data prevents the unification achieved in the other Parts of this Handbook.

Research Division, College of Engineering,
New York University,
New York, N. Y., May 10, 1956.

APPENDIX

APPLICATION SECTION

This section contains a summary of the pertinent data for design and analysis of stiffened curved plates and circular cylindrical shells which are subject to failure by instability. The information consists of instability-stress expressions and references to data in this report. A summary of the properties of structural materials may be found in Part I of the Handbook (ref. 1), in which stress-strain curves, Poisson's ratio, and cladding reduction factors are described and discussed. For ready reference table 1 contains a summary of explicit expressions for general-instability stresses of stiffened cylinders under torsion and external pressure loadings.

Panel Instability of Stiffened Curved Plates

Axial compression.- Data for stiffened flat plates are too few to permit design recommendations. However, the approach of Sechler and Dunn (ref. 46) may be employed until more data are available.

Shear.- The procedures developed by Kuhn and Griffith (ref. 47) are applicable to this case.

Combined shear and axial compression.- The stress-ratio equation

$$R_p + R_q^2 = 1 \tag{A1}$$

is applicable, in which R_p is the ratio of the applied to the allowable axial compression stress, and R_q is the corresponding quantity for the shear stresses.

General Instability of Stiffened Cylinders

Bending.- The general instability stress at the extreme compression fiber of the stiffened cylinder may be found from the expression

$$\sigma_c = CEQ_b \tag{A2}$$

in the elastic range where $C = 4.80$ for frames attached to the sheet between stiffeners, $C = 3.25$ for frames not attached to the sheet between stiffeners, and where

$$Q_b = \frac{(\rho_s \rho_f)^{3/4}(bd)^{-1/4}}{R} \tag{A3}$$

The effective sheet for use with the axial stiffeners may be found from

$$\frac{w_{e_s}}{b} = 0.5\left(\sigma_{cr_c}/\sigma_c\right)^{1/2} \tag{A4}$$

while for the frames the total width d should be used. This result is applicable to cylinders for which $L^2/Rt \geqq 100$.

For inelastic stresses use of the secant modulus appears to be applicable on the basis of the limited test data available.

Optimum design for bending.- The optimum design of a stiffened cylinder in bending requires that panel and general instability occur simultaneously. The cover thickness for this condition is related to the loading and geometry of the cylinder through the equation

$$\left(t_s/R\right)_o = \left(4C_f/\alpha_p{}^3\right)\left(\pi c^{1/2} M/R^2 Ed\right)^{1/2}\left(R/\rho_f\right) \tag{A5}$$

The optimum frame spacing may be found from

$$(d/R)_o = \left(16\pi C_f \alpha_p c^{1/4}\right)^{2/5}\left(R/\rho_f\right)^{4/5}\left(M/\pi E R^3\right)^{1/5} \tag{A6}$$

In these equations $\alpha_p = 1.15$ and C_f may be taken at 6.84×10^{-5}. The weight of the frames alone (no effective sheet included) is one-fourth that of the effective cover.

Bending of cutout cylinders.- For a cutout symmetric about the extreme compression fiber of a stiffened cylinder, the permissible bending moment may be computed utilizing the ratio

$$M/M_o = \frac{\left[\pi - (\theta/2)\right] - (1/2)\sin\theta - (1 - \cos\theta)/\left[\pi - (\theta/2)\right]}{\pi\left(\left\{\left[(1 - \cos\theta)/2\right]^{1/2}/\left[\pi - (\theta/2)\right]\right\} + \cos(\theta/2)\right)} \tag{A7}$$

in which θ is the total cutout angle and M_o is the bending moment computed from the section properties of the complete cylinder and the bending general instability stress obtained from equation (A2).

Pressure.- Explicit expressions for the general instability stress for axially and circumferentially stiffened circular cylinders in moderate- and long-length ranges are presented in table 1. For cylinders with frames but no axial stiffeners figure 15 may be used, in which all length ranges are covered.

The effective sheet to be used in computing the axial and circumferential stiffener section properties may be found from the expression

$$\frac{w_{e_s}}{b} = \frac{w_{e_f}}{d} = 0.5\left(\sigma_{cr_y}/\sigma_y\right)^{1/2}$$

Torsion.- Torsional general instability shearing stress may be computed using the explicit expressions in table 1 pertaining to the different length ranges or by using figure 16 for all length ranges. The effective sheet may be found from

$$\frac{w_{e_s}}{b} = \frac{w_{e_f}}{d} = 0.5\left(\tau_{cr}/\tau\right)^{1/2}$$

These calculations would not apply to shells in which there is a strong tension field that could introduce significant secondary stresses into the frames.

Transverse shear.- A conservative calculation for vertical-shear general instability shearing stress may be made by utilizing the relation

$$\tau_s = 0.85\tau_t \tag{A8}$$

The torsional shearing stress may be computed from table 1.

Combined torsion and bending.- The interaction relation

$$M/M_o + \left(T/T_o\right)^2 = 1 \tag{A9}$$

may be used to compute the permissible combinations of applied torsion and bending moments to a stiffened cylinder for which the separately applied torsion T_o and moment M_o would produce general instability. These loads may be computed using the instability-stress data above in conjunction with the cylinder cross-section properties.

Combined transverse shear and bending.- There is no interaction for this combination of transverse shear and bending loads. General instability occurs only for either type of loading applied alone, and, consequently, both types may be examined separately using the data presented previously.

REFERENCES

1. Gerard, George, and Becker, Herbert: Handbook of Structural Stability. Part I - Buckling of Flat Plates. NACA TN 3781, 1957.

2. Becker, Herbert: Handbook of Structural Stability. Part II - Buckling of Composite Elements. NACA TN 3782, 1957.

3. Gerard, George, and Becker, Herbert: Handbook of Structural Stability. Part III - Buckling of Curved Plates and Shells. NACA TN 3783, 1957.

4. Gerard, George: Handbook of Structural Stability. Part IV - Failure of Plates and Composite Elements. NACA TN 3784, 1957.

5. Gerard, George: Handbook of Structural Stability. Part V - Compressive Strength of Flat Stiffened Panels. NACA TN 3785, 1957.

6. Anon.: Some Investigations of the General Instability of Stiffened Metal Cylinders. I - Review of Theory and Bibliography. NACA TN 905, 1943.

7. Anon.: Some Investigations of the General Instability of Stiffened Metal Cylinders. II - Preliminary Tests of Wire-Braced Specimens and Theoretical Studies. NACA TN 906, 1943.

8. Anon.: Some Investigations of the General Instability of Stiffened Metal Cylinders. III - Continuation of Tests of Wire-Braced Specimens and Preliminary Tests of Sheet-Covered Specimens. NACA TN 907, 1943.

9. Anon.: Some Investigations of the General Instability of Stiffened Metal Cylinders. IV - Continuation of Tests of Sheet-Covered Specimens and Studies of the Buckling Phenomena of Unstiffened Circular Cylinders. NACA TN 908, 1943.

10. Anon.: Some Investigations of the General Instability of Stiffened Metal Cylinders. V - Stiffened Metal Cylinders Subjected to Pure Bending. NACA TN 909, 1943.

11. Anon.: Some Investigations of the General Instability of Stiffened Metal Cylinders. VI - Stiffened Metal Cylinders Subjected to Combined Bending and Transverse Shear. NACA TN 910, 1943.

12. Anon.: Some Investigations of the General Instability of Stiffened Metal Cylinders. VII - Stiffened Metal Cylinders Subjected to Combined Bending and Torsion. NACA TN 911, 1943.

13. Dunn, Louis G.: Some Investigations of the General Instability of Stiffened Metal Cylinders. VIII - Stiffened Metal Cylinders Subjected to Pure Torsion. NACA TN 1197, 1947.

14. Dunn, Louis G.: Some Investigations of the General Instability of Stiffened Metal Cylinders. IX - Criterions for the Design of Stiffened Metal Cylinders Subject to General Instability Failures. NACA TN 1198, 1947.

15. Hoff, N. J., and Klein, Bertram: The Inward Bulge Type Buckling of Monocoque Cylinders. I - Calculation of the Effect Upon the Buckling Stress of a Compressive Force, a Nonlinear Direct Stress Distribution, and a Shear Force. NACA TN 938, 1944.

16. Hoff, N. J., Fuchs, S. J., and Cirillo, Adam J.: The Inward Bulge Type Buckling of Monocoque Cylinders. II - Experimental Investigation of the Buckling in Combined Bending and Compression. NACA TN 939, 1944.

17. Hoff, N. J., and Klein, Bertram: The Inward Bulge Type Buckling of Monocoque Cylinders. III - Revised Theory Which Considers the Shear Strain Energy. NACA TN 968, 1945.

18. Hoff, N. J., Boley, Bruno A., and Nardo, S. V.: The Inward Bulge Type Buckling of Monocoque Cylinders. IV - Experimental Investigation of Cylinders Subjected to Pure Bending. NACA TN 1499, 1948.

19. Hoff, N. J., and Boley, Bruno A.: The Shearing Rigidity of Curved Panels Under Compression. NACA TN 1090, 1946.

20. Hoff, N. J., and Boley, Bruno A.: Stresses in and General Instability of Monocoque Cylinders With Cutouts. I - Experimental Investigation of Cylinders With a Symmetric Cutout Subjected to Pure Bending. NACA TN 1013, 1946.

21. Hoff, N. J., Boley, Bruno A., and Klein, Bertram: Stresses in and General Instability of Monocoque Cylinders With Cutouts. II - Calculation of the Stresses in a Cylinder With a Symmetric Cutout. NACA TN 1014, 1946.

22. Hoff, N. J., Boley, Bruno A., and Klein, Bertram: Stresses in and General Instability of Monocoque Cylinders With Cutouts. III - Calculation of the Buckling Load of Cylinders With Symmetric Cutout Subjected to Pure Bending. NACA TN 1263, 1947.

23. Hoff, N. J., Boley, Bruno A., and Viggiano, Louis R.: Stresses in and General Instability of Monocoque Cylinders With Cutouts. IV - Pure Bending Tests of Cylinders With Side Cutout. NACA TN 1264, 1948.

24. Hoff, N. J., and Klein, Bertram: Stresses in and General Instability of Monocoque Cylinders With Cutouts. V - Calculation of the Stresses in Cylinders With Side Cutouts. NACA TN 1435, Jan. 1948.

25. Hoff, N. J., Klein, Bertram, and Boley, Bruno A.: Stresses in and General Instability of Monocoque Cylinders With Cutouts. VI - Calculation of the Buckling Load of Cylinders With Side Cutout Subjected to Pure Bending. NACA TN 1436, March 1948.

26. Budiansky, Bernard, Seide, Paul, and Weinberger, Robert A.: The Buckling of a Column on Equally Spaced Deflectional and Rotational Springs. NACA TN 1519, 1948.

27. Gerard, G.: Minimum Weight Analysis of Compression Structures. New York Univ. Press (New York), 1956.

28. Donnell, L. H.: Stability of Thin-Walled Tubes Under Torsion. NACA Rep. 479, 1933.

29. Hoff, N. J.: Instability of Monocoque Structures in Pure Bending. Jour. Roy. Aero. Soc., vol. XLII, no. 328, April 1938, pp. 291-346.

30. Hoff, N. J.: General Instability of Monocoque Cylinders. Jour. Aero. Sci., vol. 10, No. 4, Apr. 1943, pp. 105-114, 130.

31. Brazier, L. G.: Flexure of Thin Cylindrical Shells and Other Thin Sections. Proc. Roy. Soc. (London), vol. 116, Sept. 1, 1927, pp. 104-114.

32. Flügge, W.: Die Stabilität der Kreiszylinderschale. Ing.-Archiv, Bd. 3, Dec. 1932, pp. 463-506.

33. Dschou, Dji-Djüän: Die Druckfestigkeit versteifter zylindrischer Schalen. Luftfahrtforschung, Bd. 11, Nr. 8, Feb. 6, 1935, pp. 223-234.

34. Nissen, O.: Knickversuche mit versteiften Wellblechschalen bei reiner Druckbeanspruchung. Jahrb. 1937 der deutschen Luftfahrtforschung, R. Oldenbourg (Munich), pp. I 452 - I 458.

35. Ryder, E. I.: General Instability of Semimonocoque Cylinders. Air Commerce Bull., Dept. of Commerce, vol. 9, 1938, pp. 291-346.

36. Taylor, J. L.: The Stability of a Monocoque in Compression. R. & M. No. 1679, British A.R.C. 1935.

37. Tsien, Hsue Shen: A Theory for the Buckling of Thin Shells. Jour. Aero. Sci., vol. 9, no. 10, Aug. 1942, pp. 373-384.

38. Donnell, L. H., and Wan, C. C.: Effect of Imperfections on Buckling of Thin Cylinders and Columns Under Axial Compression. Jour. Appl. Mech., vol. 17, no. 1, Mar. 1950, pp. 73-83.

39. Shanley, F. R.: Simplified Analysis of General Instability of Stiffened Shells in Pure Bending. Jour. Aero. Sci., vol. 16, no. 10, Oct. 1949, pp. 590-592.

40. Bodner, S. R.: The Analysis of the General Instability of Ring Reinforced Circular Cylindrical Shells by Orthotropic Shell Theory. Rep. 291, Polytechnic Inst. of Brooklyn, May 1955.

41. Salerno, V. L., and Levine, B.: General Instability of Reinforced Shells Under Hydrostatic Pressure. Rep. 189, Polytechnic Inst. of Brooklyn, Sept. 1951.

42. Kendrick, S.: The Buckling Under External Pressure of Circular Cylindrical Shells With Evenly Spaced, Equal Strength, Circular Ring Frames. Parts I, II, III. Reps. 211, 243, 244, Naval Construction Res. Establishment (Gt. Britain), 1955.

43. Becker, H.: General Instability of Stiffened Cylinders. NACA TN 4237, 1958.

44. Stein, Manuel, Sanders, J. Lyell, Jr., and Crate, Harold: Critical Stress of Ring-Stiffened Cylinders in Torsion. NACA Rep. 989, 1950.

45. Hayashi, Tsuyashi: Torsional Buckling of Orthogonal Anisotropic Cylinders. Proc. Eighth Int. Cong. of Theor. and Appl. Mech. (Istanbul, 1952), Univ. of Instanbul, 1953, pp. 189-190.

46. Sechler, Ernest E., and Dunn, Louis G.: Airplane Structural Analysis and Design. John Wiley & Sons, Inc., 1942.

47. Ramberg, Walter, Levy, Samuel, and Fienup, Kenneth L.: Effect of Curvature on Strength of Axially Loaded Sheet Stringer Panels. NACA TN 944, 1944.

48. Kuhn, Paul, and Griffith, George E.: Diagonal Tension in Curved Webs. NACA TN 1481, 1947.

49. Melcon, M. A., and Ensrud, A. F.: Analysis of Stiffened Curved Panels Under Shear and Compression. Jour. Aero. Sci., vol. 20, no. 2, Feb. 1953, pp. 111-119, 126. (Errata issued vol. 21, no. 6, June 1954, p. 427.)

50. Peterson, James P.: Experimental Investigation of Stiffened Circular Cylinders Subjected to Combined Torsion and Compression. NACA TN 2188, 1950.

51. Heck, O. S.: The Stability of Orthotropic Elliptic Cylinders in Pure Bending. NACA TM 834, 1937.

52. Wignot, J. E., Combs, Henry, and Ensrud, A. F.: Analysis of Circular Shell-Supported Frames. NACA TN 929, 1944.

53. Timoshenko, S.: Theory of Elastic Stability. First ed., McGraw-Hill Book Co., Inc., 1936.

54. Nash, W. A.: General Instability of Ring-Reinforced Cylindrical Shells Subject to Hydrostatic Pressure. Proc. Second U. S. Nat. Cong. Appl. Mech. (Univ. Mich., Ann Arbor, 1954), A.S.M.E., 1955, pp. 359-368.

55. Levy, M.: Liouville's Journal of Pure and Applied Mathematics, ser. 3, vol. 10, 1884, p. 5.

56. Batdorf, S. B., Stein, Manuel, and Schildcrout, Murry: Critical Stress of Thin-Walled Cylinders in Torsion. NACA TN 1344, 1947.

TABLE 1

THEORETICAL GENERAL INSTABILITY STRESSES OF ORTHOTROPIC CIRCULAR CYLINDERS

[Results are based on the assumption that spacings of longitudinal stiffeners and circumferential frames are uniform and small enough to permit assumption that cylinder acts as orthotropic shell]

Loading	Moderate-length cylinders	Long cylinders
Bending	$\sigma_c = gE\left(I_f t\right)^{1/2} \Big/ Rt_s$ $g = 4.80\left[(b/d)\left(\rho_s/\rho_f\right)\left(t_s/t_f\right)^2\left(\rho_s/b\right)^2\right]^{1/4}$	
External radial or hydrostatic pressure	$\sigma_y = 5.51E\left(\frac{t_s}{t_f}\right)^{1/4}\left(\frac{\rho_f}{R}\right)^{1/2}\left(\frac{R}{L}\right)$	$\sigma_y = 3E\left(\rho_f/R\right)^2$
Torsion	$\tau = 3.46\left(\frac{t_s}{t}\right)^{3/8}\left(\frac{I_f}{R^2 t}\right)^{5/8}\left(\frac{R}{L}\right)^{1/2}$	$\tau = 1.754\left(\frac{t_s}{t}\right)^{1/4}\left(\frac{I_f}{R^2 t}\right)^{3/4}$

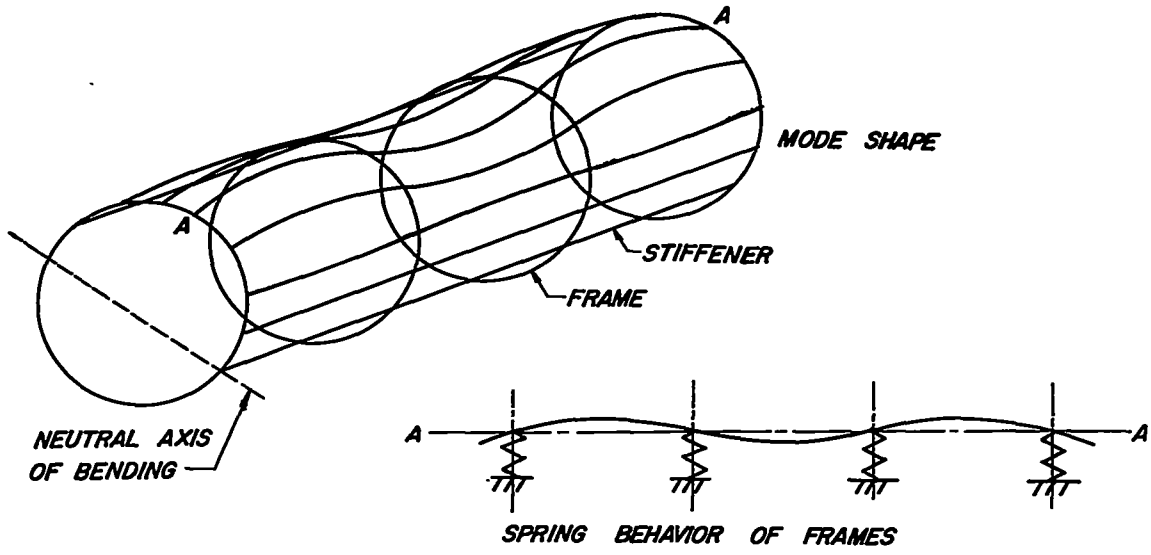

(a) Panel instability.

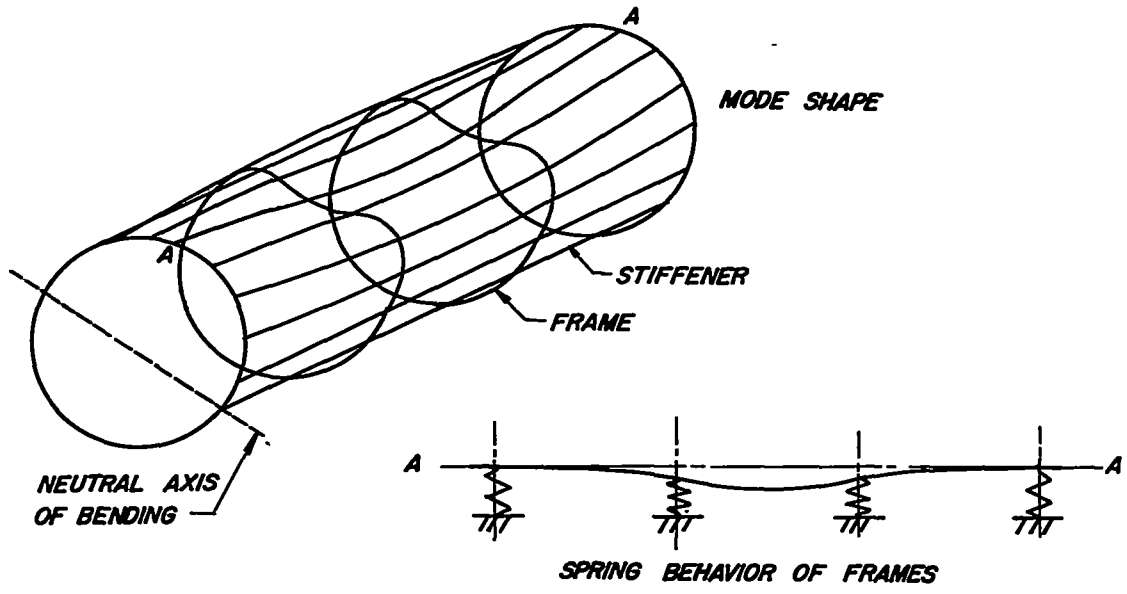

(b) General instability.

Figure 1.- Mode shapes for panel and general instability of stiffened cylinders in bending.

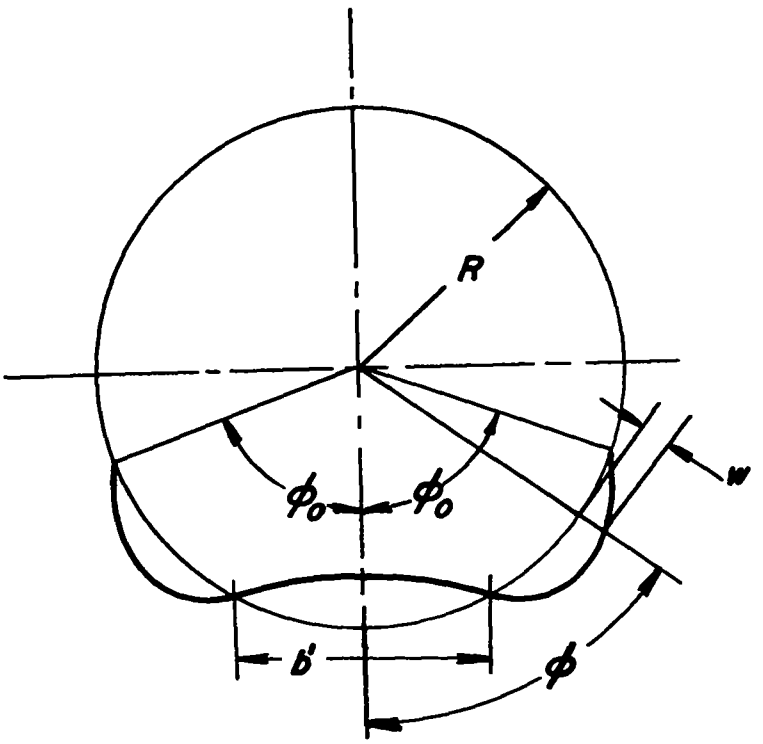

(a) Deflected shape of ring.

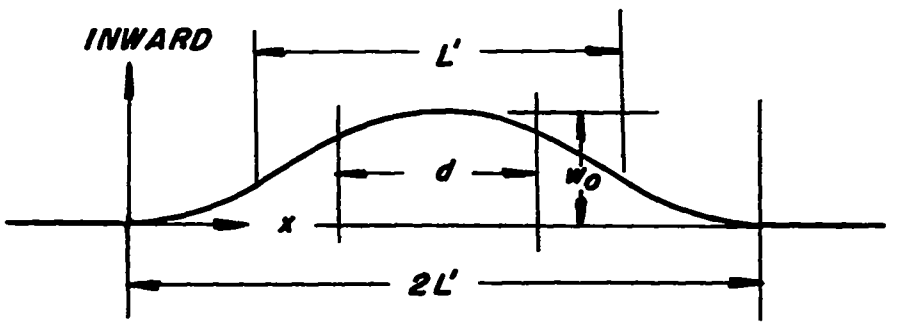

(b) Deflected shape of stiffener.

Figure 2.- Geometry of inward-bulge buckle.

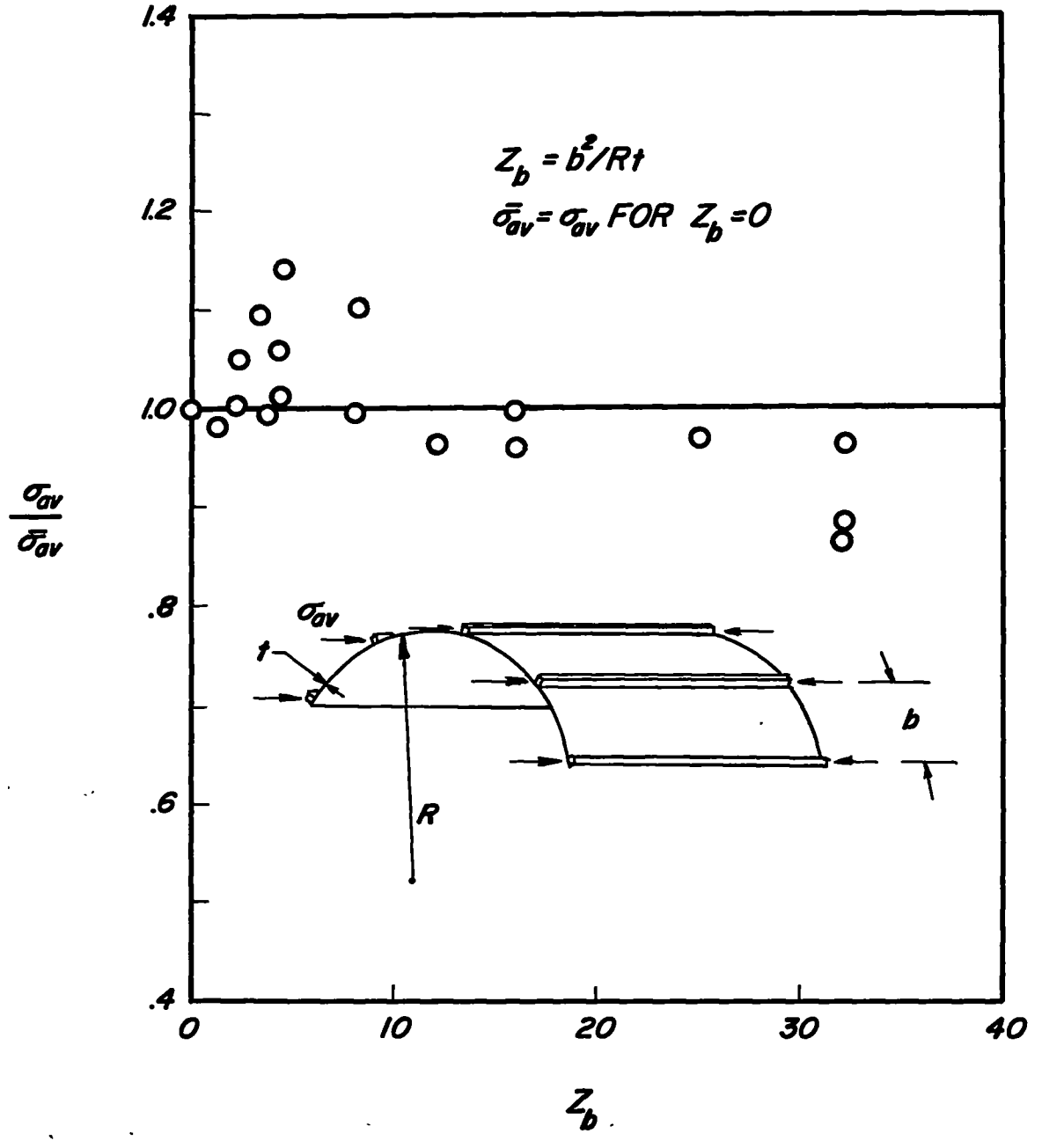

Figure 3.- Effect of curvature on axial compressive strength of stiffened panels (data of ref. 47).

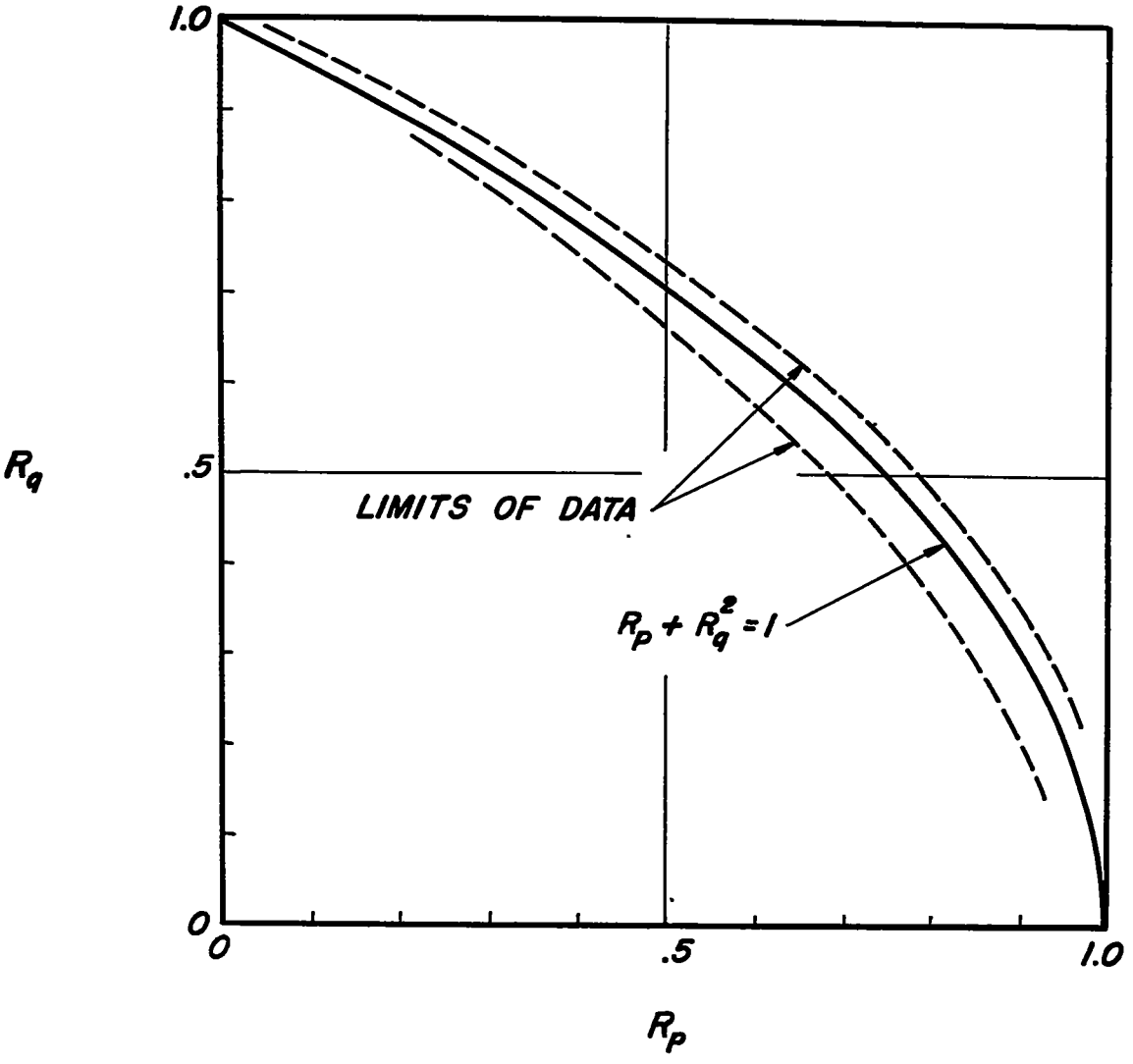

Figure 4.- Interaction curve for combined axial and shear loads on stiffened curved panels (data of ref. 50).

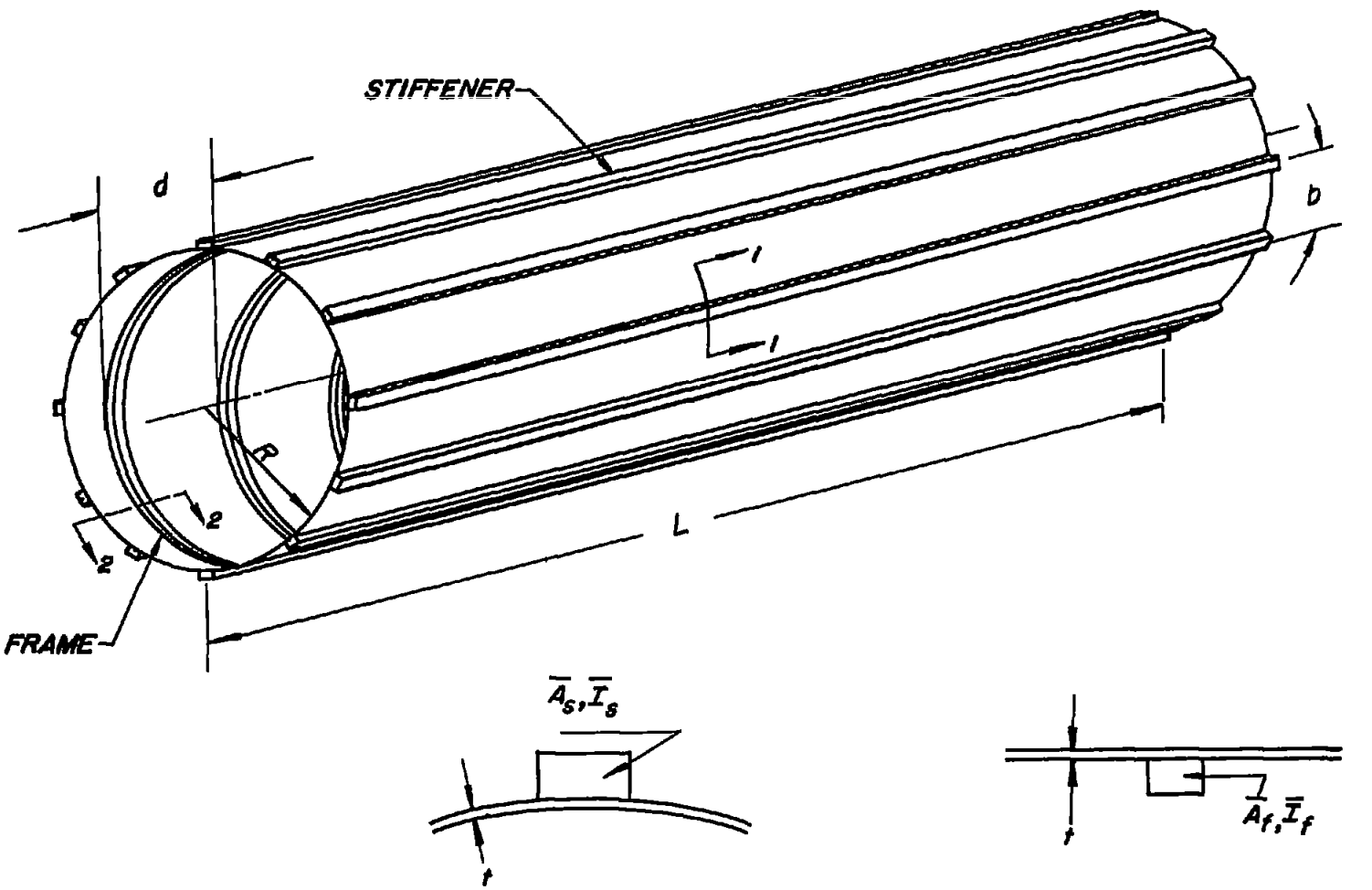

Figure 5.- Geometry of idealized stiffened circular cylinder.

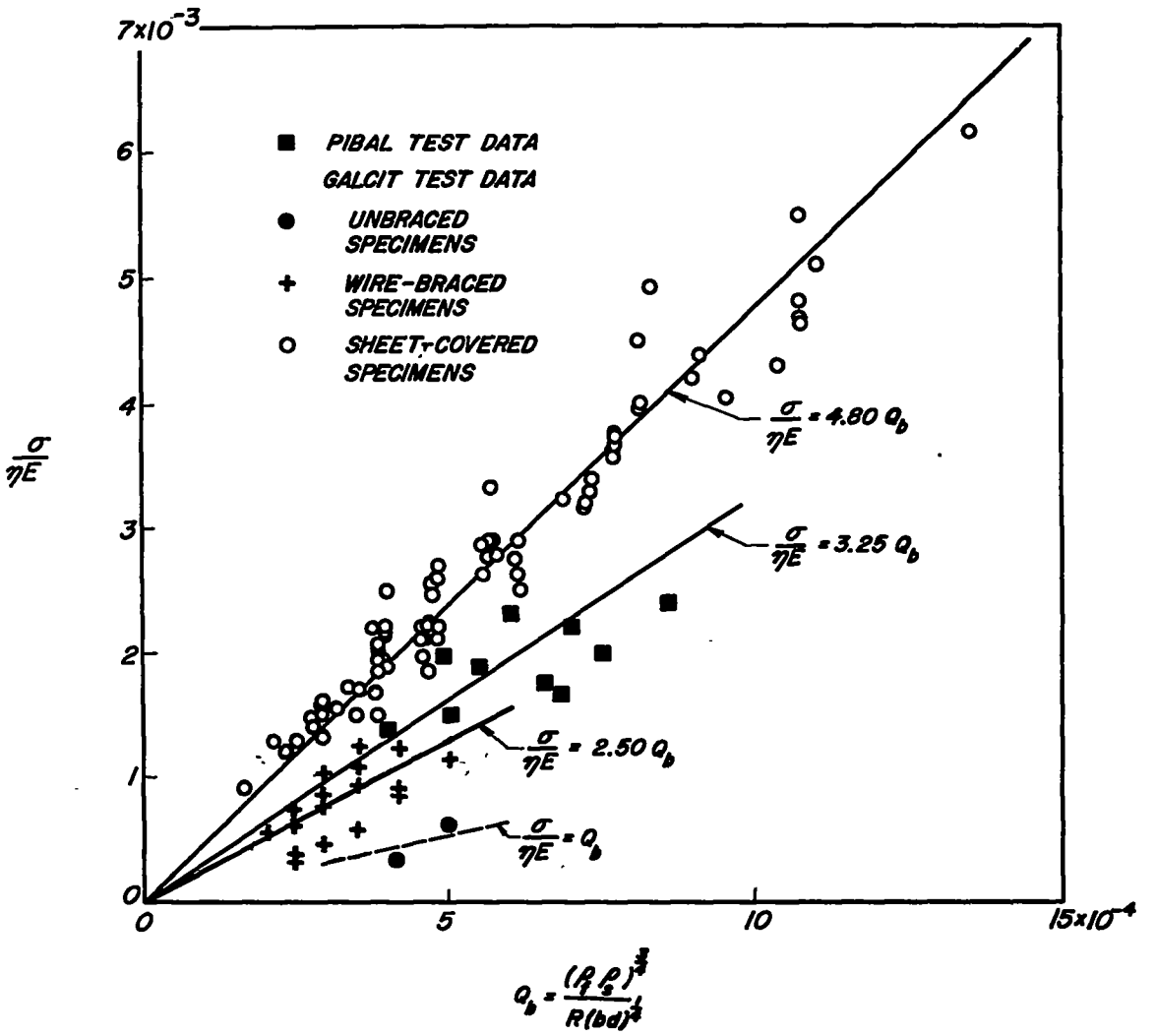

Figure 6.- Test data and empirical curves for bending general instability.

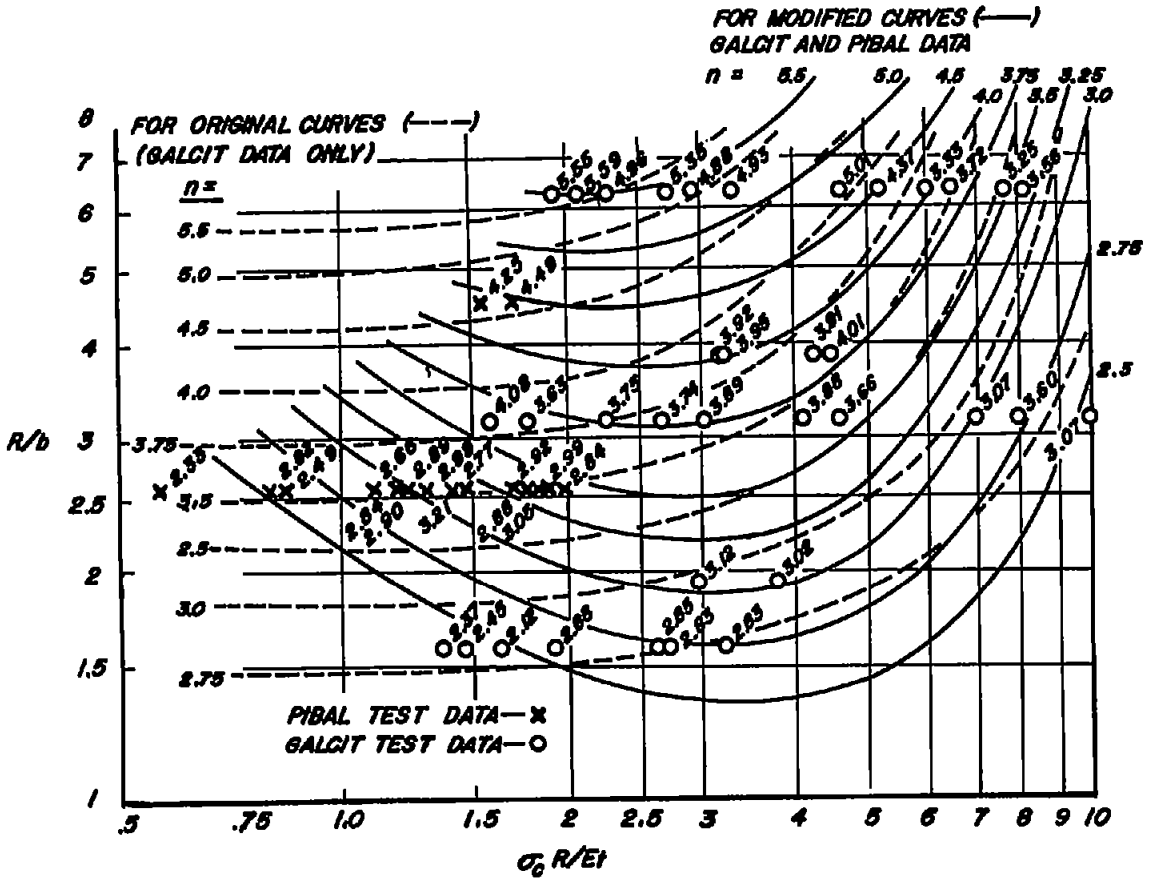

Figure 7.- Empirical chart relating cylinder geometry and buckle parameters for bending general instability.

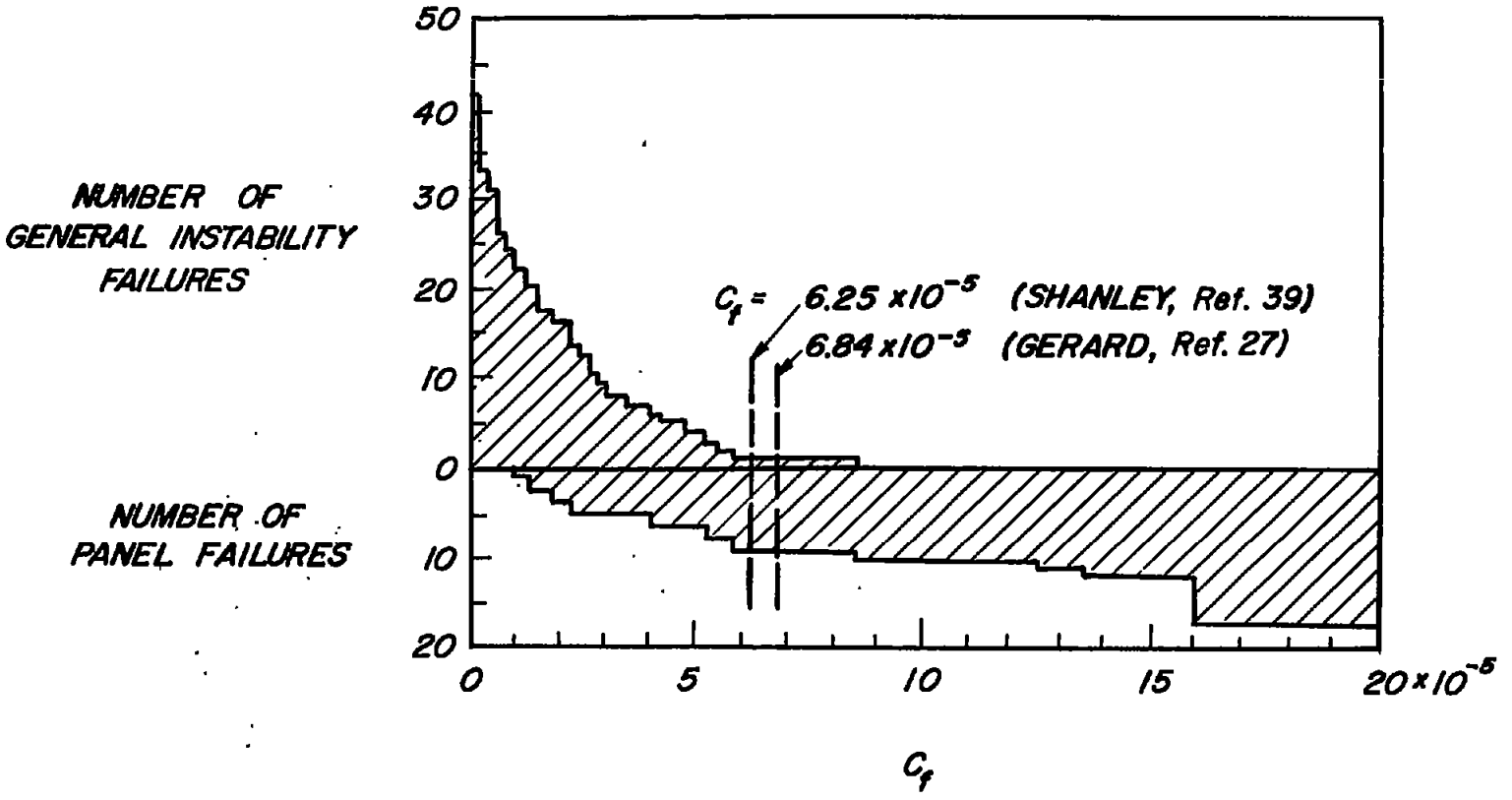

Figure 8.- Relation between type of failure and frame stiffness parameter.

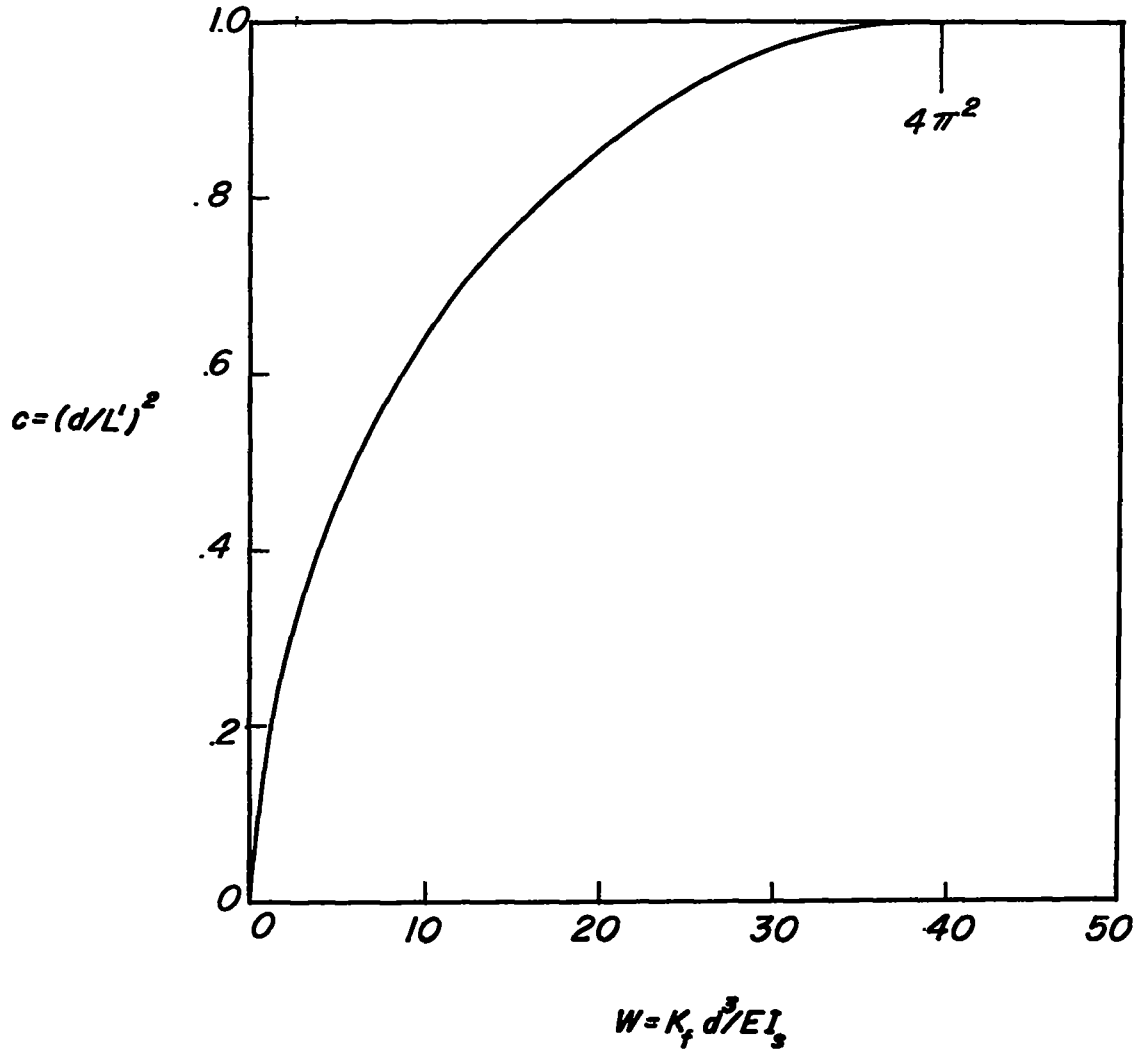

Figure 9.- Stiffener fixity coefficient as a function of frame spring constant.

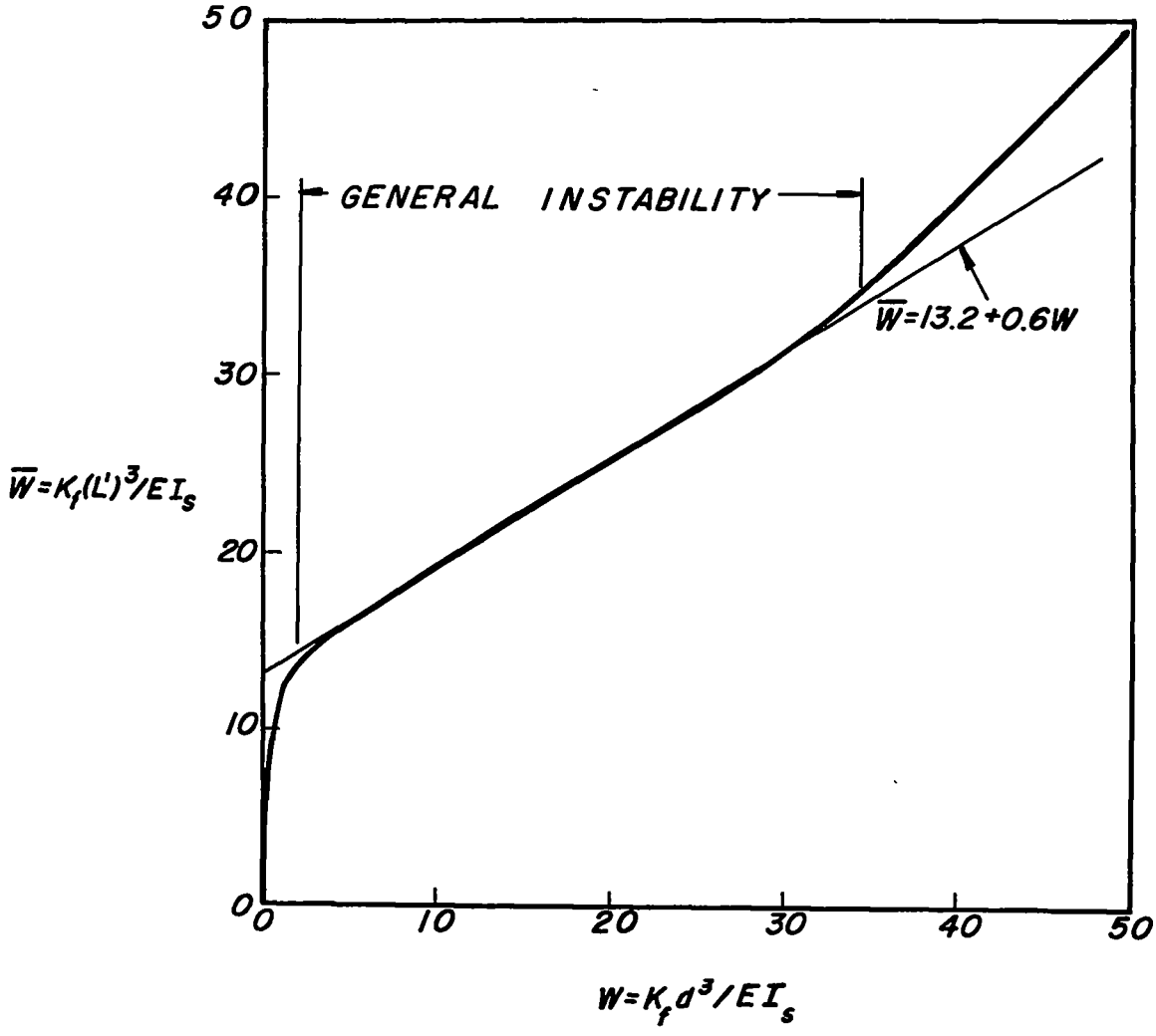

Figure 10.- Revised plot of figure 9.

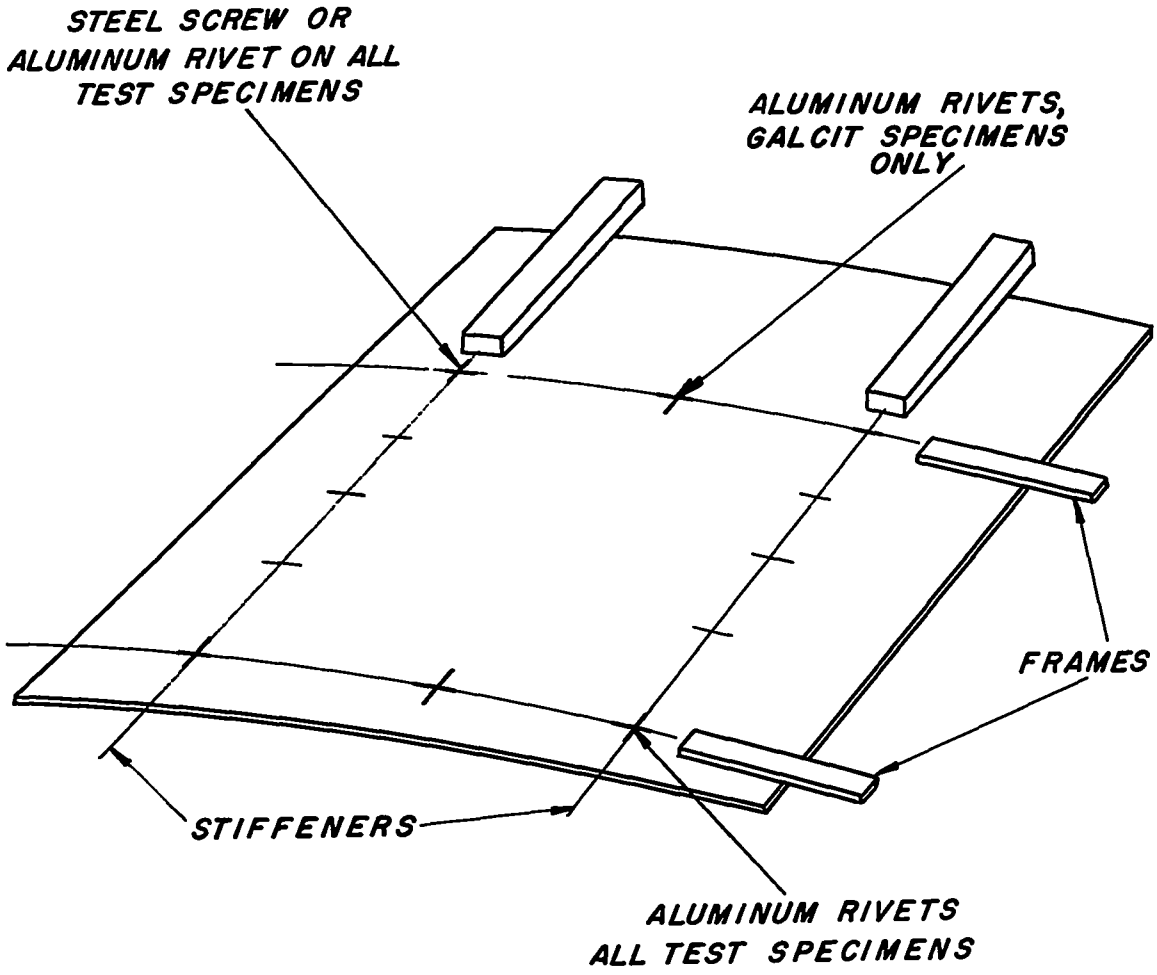

Figure 11.- Locations of connections on GALCIT and PIBAL test cylinders.

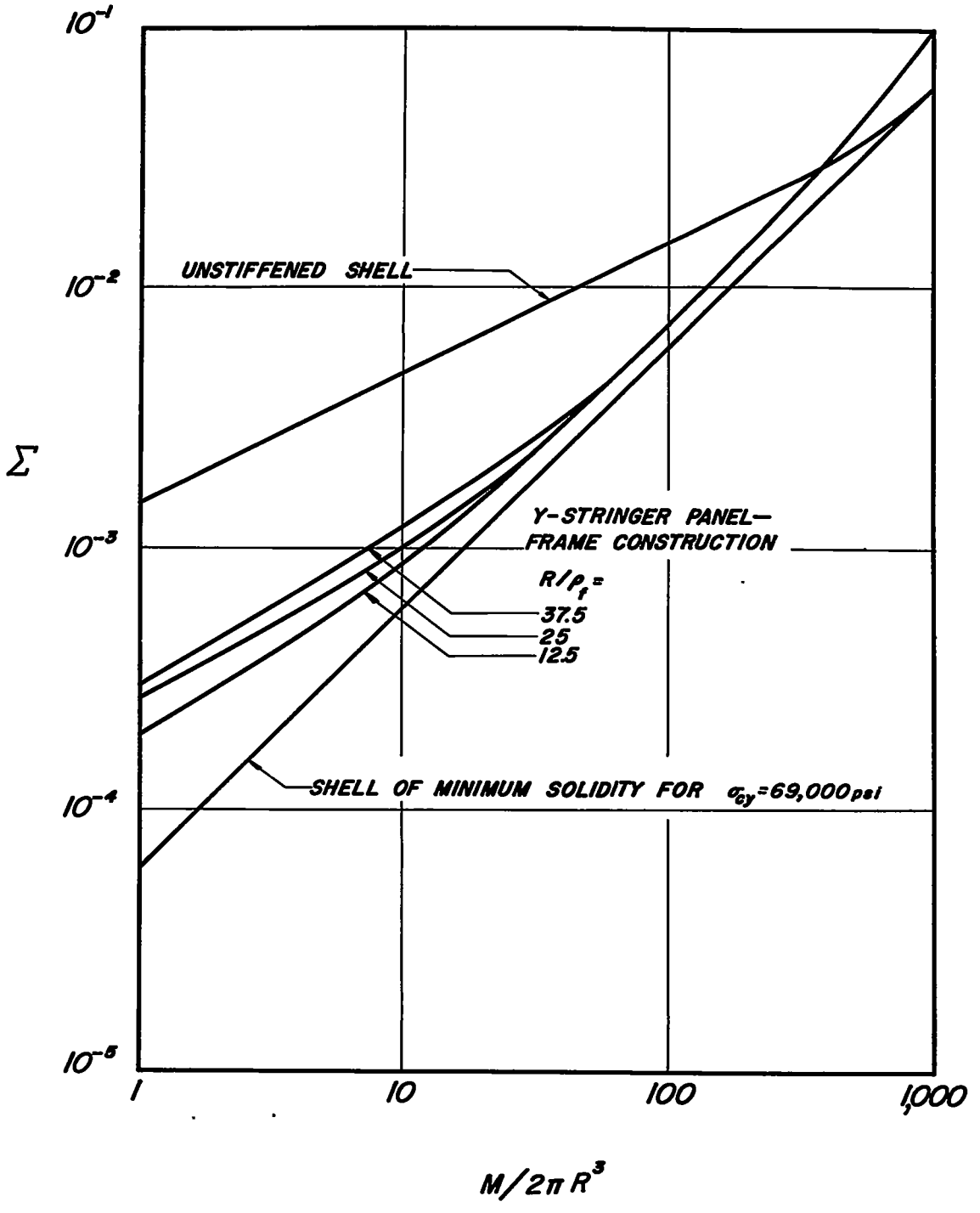

Figure 12.- Comparative efficiency chart for circular cylinders in bending.

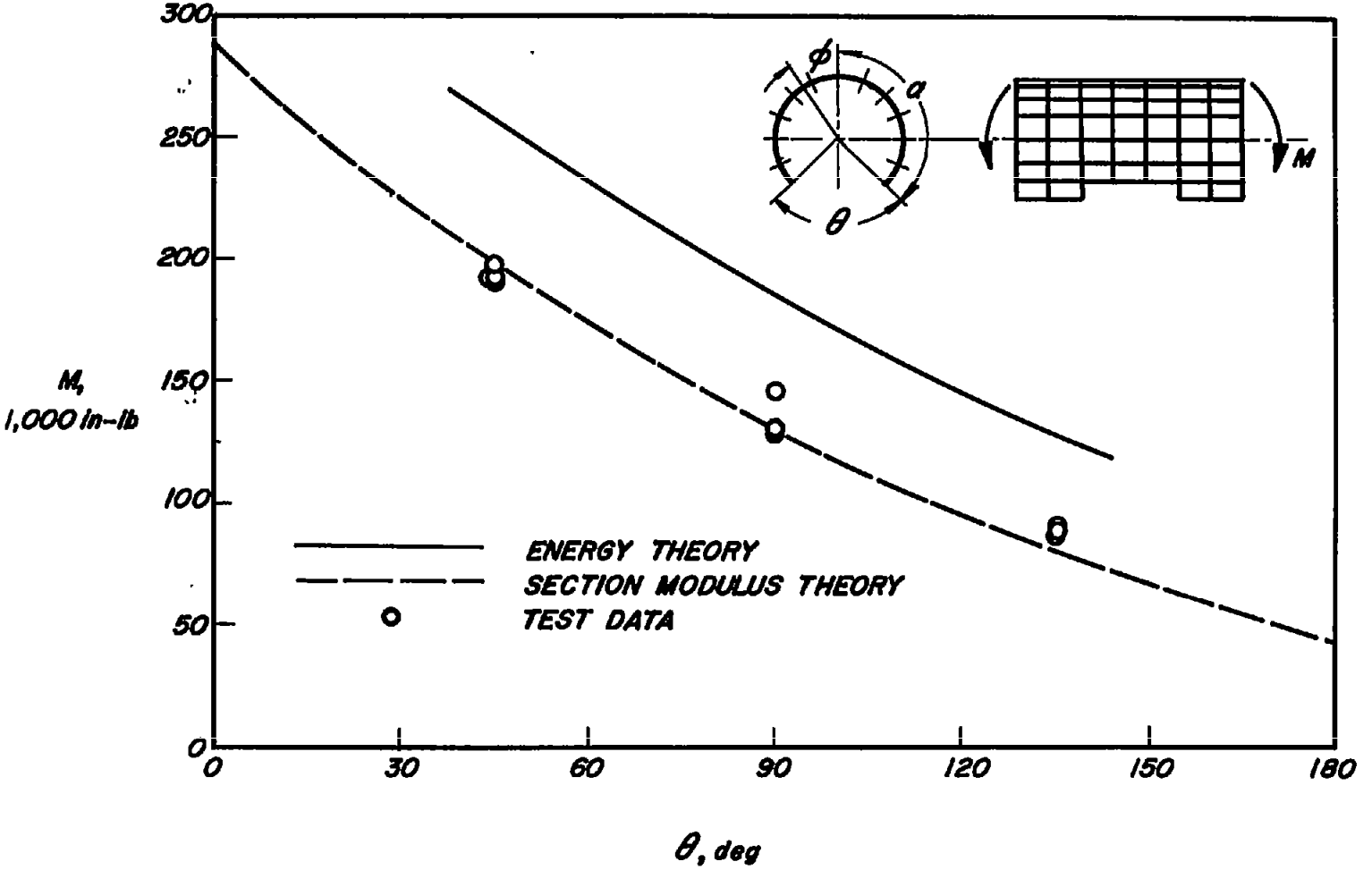

Figure 13.- Bending strengths of stiffened circular cylinders with symmetric cutouts.

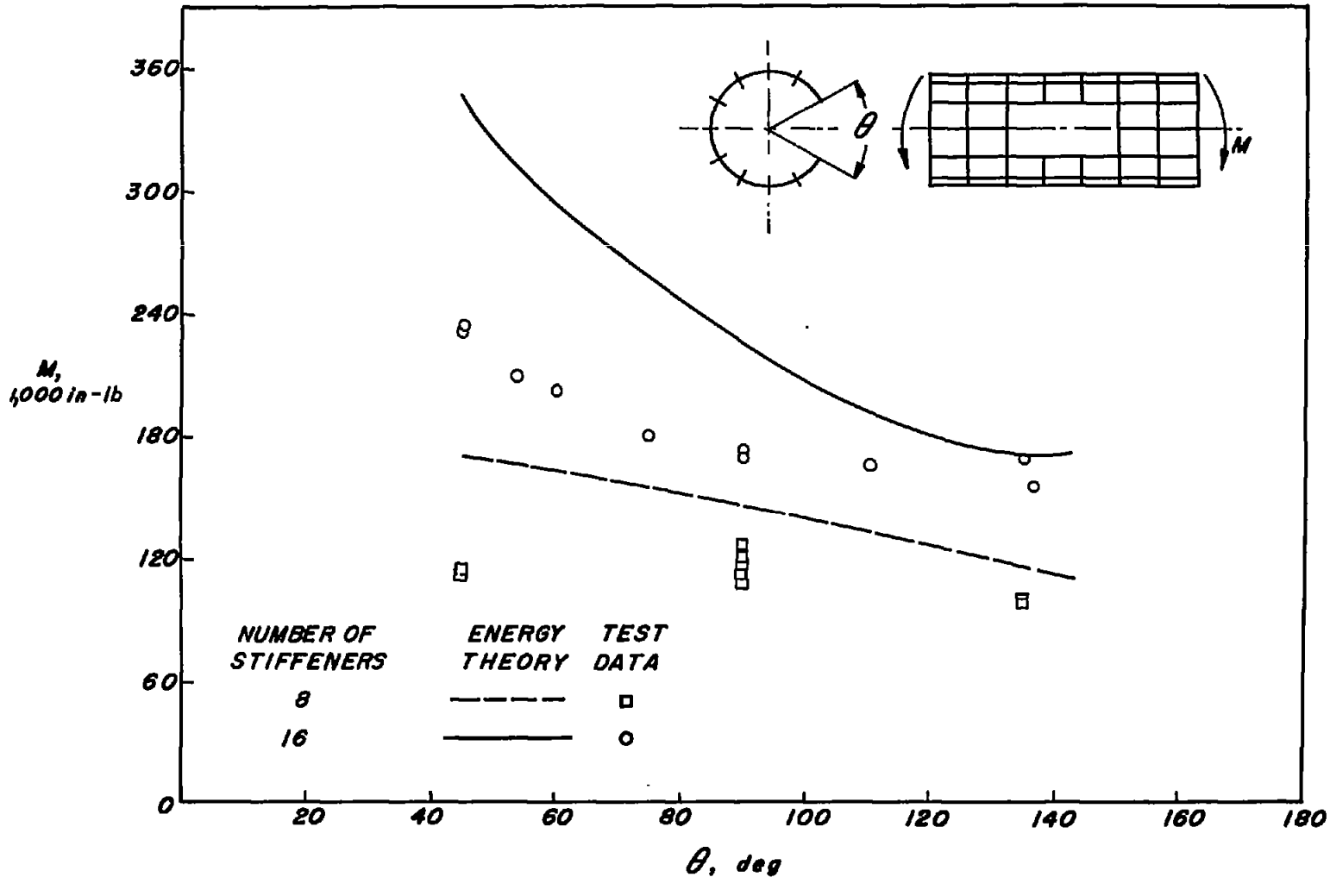

Figure 14.- Bending strengths of stiffened circular cylinders with side cutouts.

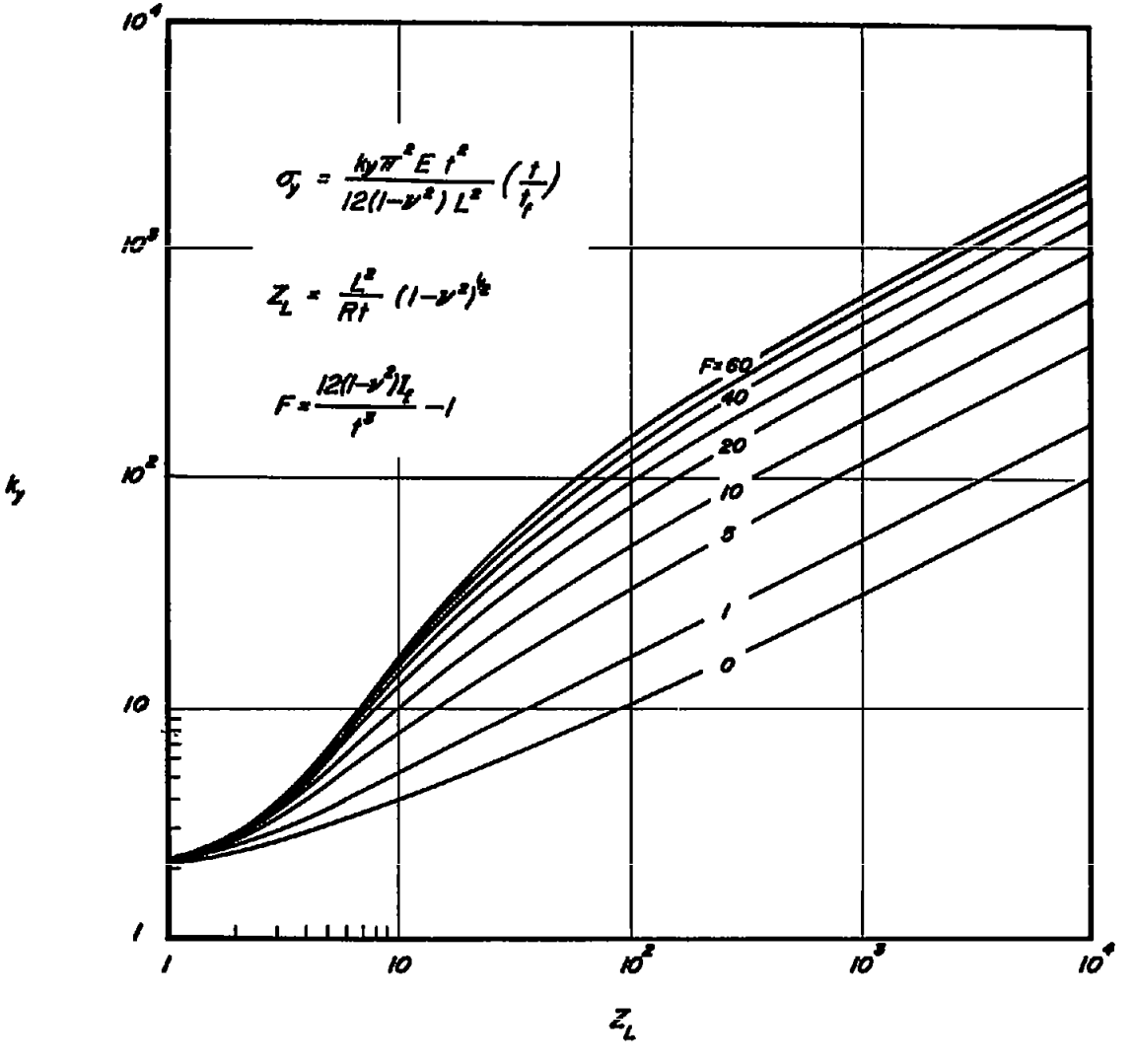

Figure 15.- External pressure general instability coefficient of ring-stiffened cylinders as a function of curvature and frame parameters.

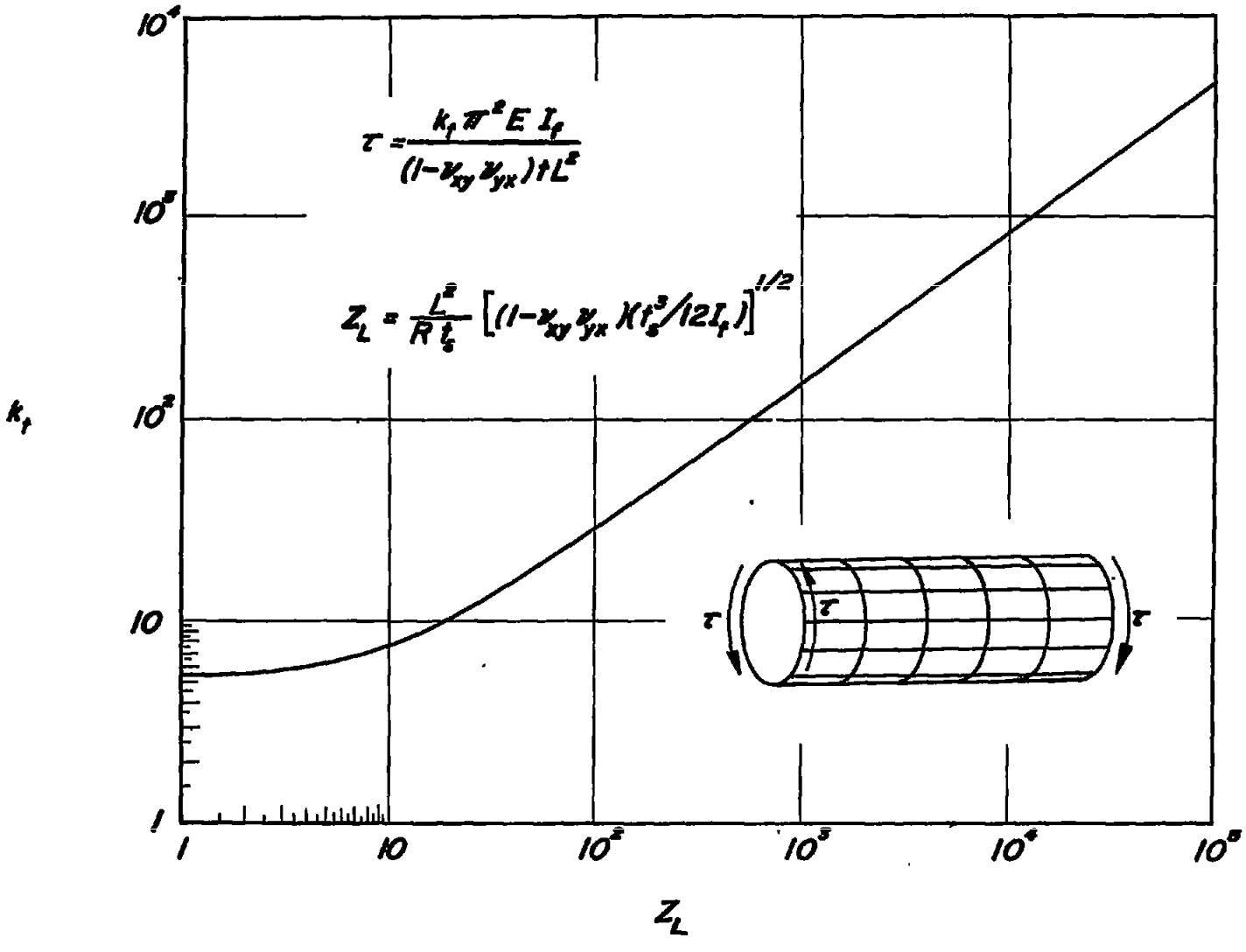

Figure 16.- Torsion general instability coefficient of stiffened cylinders as a function of generalized curvature parameter.

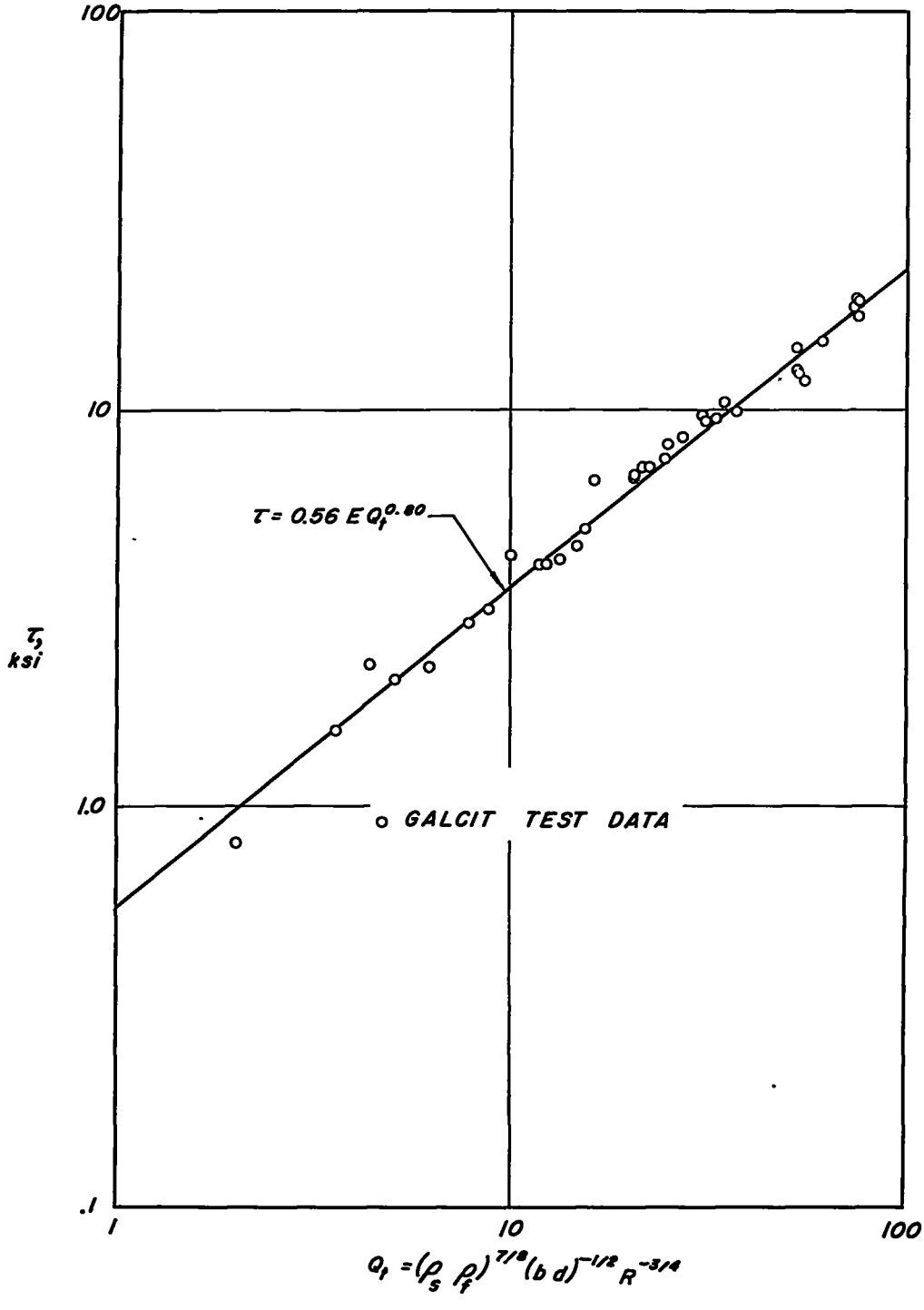

Figure 17.- Torsion general instability stress as a function of the GALCIT empirical parameter (data of ref. 13).

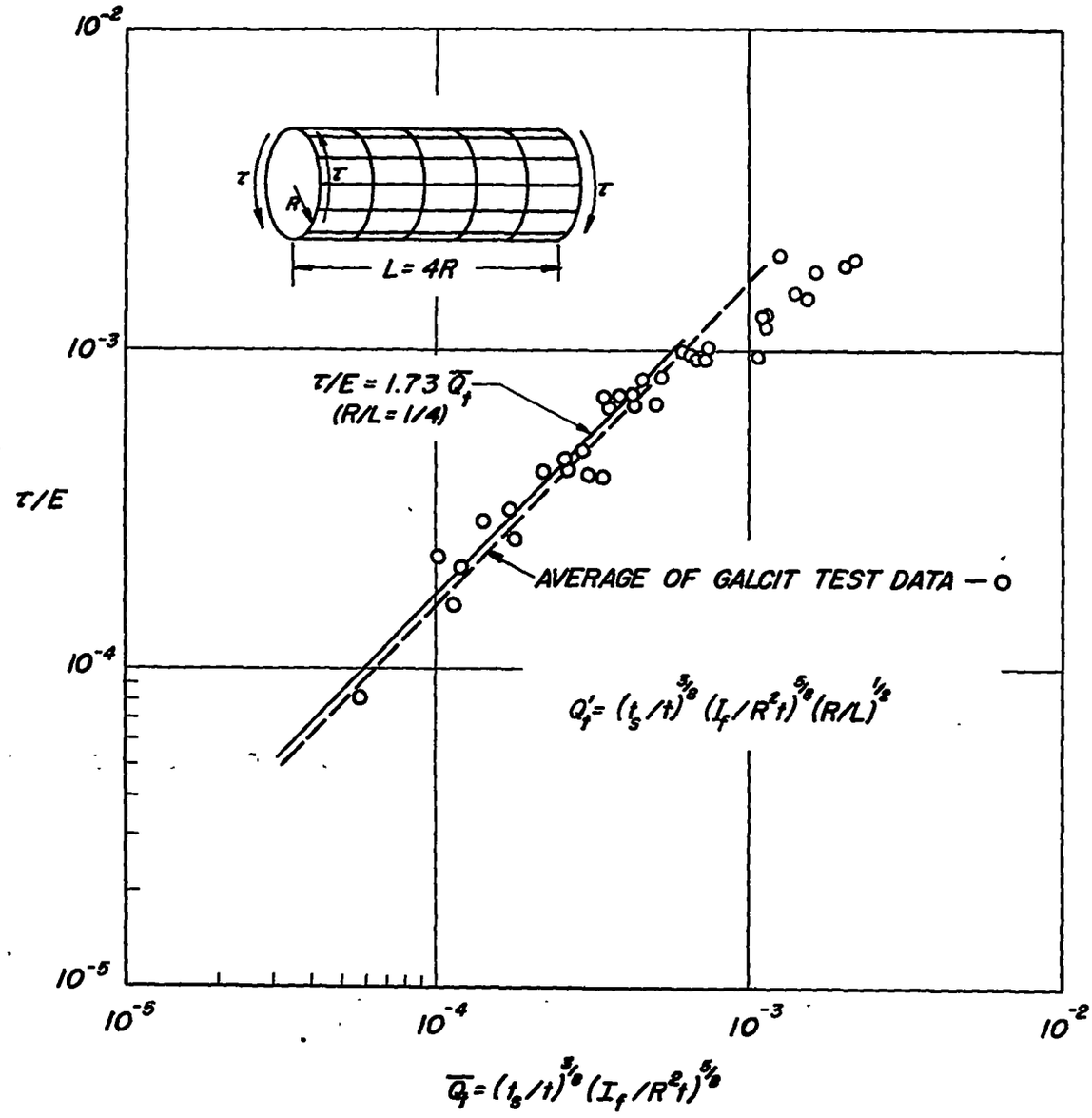

Figure 18.- Comparison of test data with theory for torsion general instability for constant values of R/L.

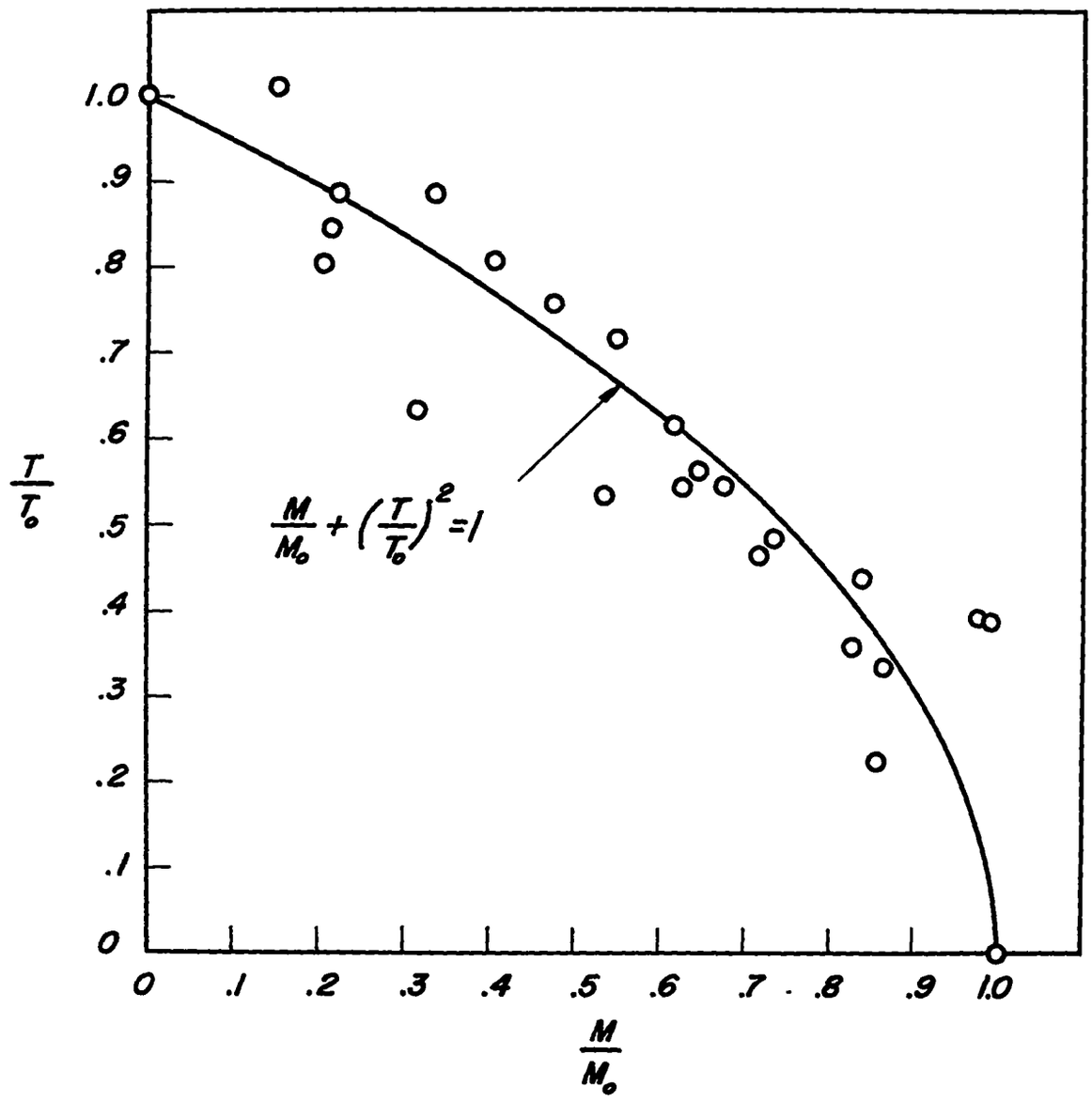

Figure 19.- Interaction curve for combined bending and torsion general instability of stiffened circular cylinders (data of ref. 12).